

ORNL REPORT

ORNL/TM-2014/36
Unlimited Release
Printed March 2014

A hyper-spherical adaptive sparse-grid method for high-dimensional discontinuity detection

G. Zhang, C. G. Webster, M. Gunzburger and J. Burkardt

Prepared by
Department of Computational and Applied Mathematics
Computer Science and Mathematics Division
Oak Ridge National Laboratory
One Bethel Valley Road, Oak Ridge, Tennessee 37831

The Oak Ridge National Laboratory is operated by UT-Battelle, LLC,
for the United States Department of Energy under Contract DE-AC05-00OR22725.
Approved for public release; further dissemination unlimited.

DOCUMENT AVAILABILITY

Reports produced after January 1, 1996, are generally available free via the U.S. Department of Energy (DOE) Information Bridge.

Web site <http://www.osti.gov/bridge>

Reports produced before January 1, 1996, may be purchased by members of the public from the following source.

National Technical Information Service

5285 Port Royal Road

Springfield, VA 22161

Oak Ridge, TN 37831

Telephone 703-605-6000 (1-800-553-6847)

TDD 703-487-4639

Fax 703-605-6900

E-mail info@ntis.gov

Web site <http://www.ntis.gov/support/ordernowabout.htm>

Reports are available to DOE employees, DOE contractors, Energy Technology Data Exchange (ETDE) representatives, and International Nuclear Information System (INIS) representatives from the following source.

Office of Scientific and Technical Information

P.O. Box 62

Oak Ridge, TN 37831

Telephone 865-576-8401

Fax 865-576-5728

E-mail reports@osti.gov

Web site <http://www.osti.gov/contact.html>

NOTICE

This report was prepared as an account of work sponsored by an agency of the United States Government. Neither the United States Government, nor any agency thereof, nor any of their employees, nor any of their contractors, subcontractors, or their employees, make any warranty, express or implied, or assume any legal liability or responsibility for the accuracy, completeness, or usefulness of any information, apparatus, product, or process disclosed, or represent that its use would not infringe privately owned rights. Reference herein to any specific commercial product, process, or service by trade name, trademark, manufacturer, or otherwise, does not necessarily constitute or imply its endorsement, recommendation, or favoring by the United States Government, any agency thereof, or any of their contractors or subcontractors. The views and opinions expressed herein do not necessarily state or reflect those of the United States Government, any agency thereof, or any of their contractors.

Printed in the United States of America. This report has been reproduced directly from the best available copy.



A HYPER-SPHERICAL ADAPTIVE SPARSE-GRID METHOD FOR HIGH-DIMENSIONAL DISCONTINUITY DETECTION

Guannan Zhang^{*} Clayton G. Webster[†] Max Gunzburger[‡] John Burkardt[§]

Abstract. This work proposes and analyzes a hyper-spherical adaptive hierarchical sparse-grid method for detecting jump discontinuities of functions in high-dimensional spaces is proposed. The method is motivated by the theoretical and computational inefficiencies of well-known adaptive sparse-grid methods for discontinuity detection. Our novel approach constructs a function representation of the discontinuity hyper-surface of an N -dimensional discontinuous quantity of interest, by virtue of a hyper-spherical transformation. Then, a sparse-grid approximation of the transformed function is built in the hyper-spherical coordinate system, whose value at each point is estimated by solving a one-dimensional discontinuity detection problem. Due to the smoothness of the hyper-surface, the new technique can identify jump discontinuities with significantly reduced computational cost, compared to existing methods. Moreover, hierarchical acceleration techniques are also incorporated to further reduce the overall complexity. Rigorous error estimates and complexity analyses of the new method are provided as are several numerical examples that illustrate the effectiveness of the approach.

Key words. discontinuity detection, hyper-spherical coordinate system, adaptive sparse grid, rare events, hierarchical acceleration

1. Introduction. Numerical approximation is an important tool used to define solution techniques for physical, biological, economic systems. In simulations of such systems, the relationship between the inputs that drive the system and the outputs, i.e., the system responses, are described by a multivariate function which is usually the target of the numerical approximation. Often the target function exhibits jump discontinuities, which have motivated many research efforts devoted to discontinuity detection. Traditionally, discontinuity detection has been associated with capturing jump discontinuities of a process with respect to temporal and/or spatial variables; thus, most efforts are restricted to low-dimensional problems. However, high-dimensional discontinuity detection is of significant importance to cases where the system outputs depend on a large number of input variables. For example, this challenge arises in uncertainty quantification (UQ), where physical systems with uncertainties are described by stochastic partial differential equations (SPDEs) with random input data. It is well known that an output of interest derived from the solution of an SPDE may depend on a large number of random variables that result from the characterization of the uncertainties. Outputs of interest often contain jump

^{*}Computer Science and Mathematics Division, Oak Ridge National Laboratory, One Bethel Valley Road, P.O. Box 2008, MS-6164, Oak Ridge, TN 37831-6164 (zhangg@ornl.gov)

[†]Computer Science and Mathematics Division, Oak Ridge National Laboratory, One Bethel Valley Road, P.O. Box 2008, MS-6164, Oak Ridge, TN 37831-6164 (webstercg@ornl.gov)

[‡]Department of Scientific Computing, 400 Dirac Science Library, Florida State University, Tallahassee, FL 32306-4120 (mgunzburger@fsu.edu)

[§]Department of Scientific Computing, 400 Dirac Science Library, Florida State University, Tallahassee, FL 32306-4120 (jburkardt@fsu.edu)

discontinuities, sometimes because of singular or other irregular behavior in random coefficients, and forcing terms, in the SPDE, but can even occur if the input data are smooth, or because the output of interest itself is defined in terms on non-smooth functions, e.g., indicator functions. Another setting where high-dimensional discontinuity detection is of importance is in optimization and control problems where again, the controls are characterized using a large number of parameters and discontinuous cost functionals often arise. Therefore, the development of novel, accurate, and efficient numerical techniques for approximating high-dimensional discontinuous functions is highly desired in the UQ, control, and other communities.

A straightforward approach to resolving the challenges faced when approximating discontinuous functions is to first subdivide the high-dimensional parameter domain into several subdomains, in each of which the target function is continuous or even smoother. Then, in each subdomain, construct a piecewise continuous polynomial approximation using well-known methods such as sparse-grid interpolants [5, 11, 12] or even orthogonal polynomial expansions [16, 17]. Obviously, these approaches require that the boundaries of the subdomains follow the discontinuity manifolds of the target function. Although such approaches are conceptually easy to understand, they are severely challenged numerically, when one requires accurate representations of the detected discontinuities in high dimensions. Moreover, in applications, the evaluation of the target function often involves expensive simulations of complex models, e.g., the repeated execution of a computationally demanding solver for a system of PDEs. In this case, efficiency is another important criterion to assess the performance of an algorithm for high-dimensional discontinuity detection. Recently, several attempts have been made to alleviate the challenges in locating discontinuities. In [1, 2], a polynomial annihilation approach, originally developed for one and two-dimensional edge detection, was extended to solve problems in high dimensions. However, such methods rely on the evaluation of the target function based on a set of local tensor-product grids, so that the number of function evaluations grows exponentially as the dimension increases. Improvements were made in [8] by incorporating the adaptive hierarchical sparse-grid (AHSG) approximation, in order to reduce the computational cost. The AHSG method has been demonstrated [4, 5, 15, 19, 20] to be effective in approximating high-dimensional smooth functions, but the effectiveness of the AHSG approximations inextricably relies on the smoothness of the target function. When approximating a discontinuous function, mesh refinement is invariable needed in the vicinity of discontinuities, resulting in a significantly deterioration in the sparsity of the grid, i.e., using an AHSG method, a discontinuity of an N -dimensional function, which occurs across an $N - 1$ dimensional hyper-surface, has to be approximated using a “dense” grid, as illustrated by Example 3.1 in §3.2. This disadvantage dramatically limits the applicability of AHSG methods for high-dimensional discontinuity detection.

To combat these challenges, in this work, we propose a hyper-spherical adaptive hierarchal sparse-grid (HS-AHSG) method that, for functions in high dimensions con-

taining jump discontinuities, achieves the desired performance and retains most of the grid sparsity of AHSG methods, that are known to be effective for the approximation of smooth functions. The basic idea is to approximate the discontinuity hyper-surface directly instead of approximating the discontinuous function, motivated by observing that the hyper-surface itself is often continuous or even smoother. Therefore, the number of grid points needed to approximate the hyper-surface can be significantly reduced compared to existing AHSG methods. To achieve this, the first step is to define a function representation of the $N - 1$ -dimensional discontinuity hyper-surface. Under a mild assumption about its geometry, the hyper-surface is transformed to a function in a hyper-spherical coordinate system. Note that the transformed function is defined in the subspace constituted by $N - 1$ angle coordinates; the function value at a certain point is the Euclidean distance between the origin of the hyper-spherical coordinate system and the discontinuity along the direction determined by the $N - 1$ angles. The next step is to develop an approach to evaluate the transformed function, i.e., calculating the desired Euclidean distance at a given point. Fortunately, this is relatively easy and trivial to implement because it reduces to an one-dimensional discontinuity detection problem along each of the directions determined by the $N - 1$ angles. Many existing techniques can be used to fulfill this relatively straight-forward task, such as the polynomial annihilation or an existing AHSG method. In particular, if the discontinuous function has a *characteristic property* (defined in §2), e.g. a characteristic function, then root-finding methods can be applied as well. Based on the above two steps, an HS-AHSG approximation of the discontinuous hyper-surface can be constructed in the $N - 1$ -dimensional subspace, with the use of the hyper-spherical coordinate system.

The efficiency of our algorithm is characterized by the total number of function evaluations required by the HS-AHSG approximation. Thus, the computational complexity is not the number of sparse-grid points, but is the sum of the number of function evaluations consumed by all the one-dimensional discontinuity detection problems. Taking the bisection method as an example, the number of iterations required to achieve a prescribed accuracy is determined by the length of initial search interval. Thus, to further improve the computational efficiency, we incorporate the hierarchal acceleration technique proposed in [9] into the HS-AHSG framework. Specifically, the HS-AHSG approximation on a coarse sparse grid is used to predict the value of the transformed function at the new added points on a finer sparse grid. In this way, the length of the initial search interval for each bisection simulation is significantly reduced, as well as the necessary number of search iterations.

The main contributions of this paper are summarized as follows.

- A comprehensive framework for the HS-AHSG method for high-dimensional discontinuity detection is constructed .
- The performance of several approaches for the evaluation of the transformed function are investigated.

- The computational efficiency of the HS-AHSG method is improved by incorporating hierarchical acceleration techniques.
- Rigorous error estimates and complexity analyses are provided for the proposed algorithms.
- Numerical examples illustrating the theoretical results and the efficiency of HS-AHSG methods.

The rest of the paper is organized as follows. Specific problem definition and preliminary notions are discussed in §2. In §3, the AHSG method is briefly reviewed and an example is given to illustrate its disadvantages when attempting to detect, even moderate dimensional discontinuities. Our main results are given in §4. The function representation of the discontinuity hyper-surface and its evaluation are discussed in §4.1 and §4.2, respectively; the basic and accelerated HS-AHSG algorithms are presented in §4.3 and §4.4, respectively. Rigorous error estimates and complexity analyses are conducted in §4.5. Extensive numerical tests and comparisons are given in §5; the results are shown to be consistent with the derived theoretical estimates. Finally, concluding remarks are given in §6.

2. Problem setting. Let Γ denote an open bounded domain in \mathbb{R}^N , $N \geq 1$, and let $\partial\Gamma$ denote its boundary. We assume there exists an $N - 1$ dimensional hyper-surface in Γ , denoted by γ , separating the domain Γ into disjoint open subdomains Γ_1 and Γ_2 , such that $\Gamma = \Gamma_1 \cup \gamma \cup \Gamma_2$, $\bar{\Gamma}_1 \cap \bar{\Gamma}_2 = \gamma$, and $\Gamma_1 \cap \gamma = \Gamma_2 \cap \gamma = \Gamma_1 \cap \Gamma_2 = \emptyset$. We observe that the volume of γ in \mathbb{R}^N is zero and Γ_1 and Γ_2 are both open along γ . The boundaries of Γ_1 and Γ_2 are given by $\partial\Gamma_1 = (\partial\Gamma \cup \bar{\Gamma}_1) \cup \gamma$ and $\partial\Gamma_2 = (\partial\Gamma \cup \bar{\Gamma}_2) \cup \gamma$, respectively. We consider the generic N -dimensional discontinuous function $f(\mathbf{y}) : \Gamma \rightarrow \mathbb{R}$ given by

$$f(\mathbf{y}) = \begin{cases} f_1(\mathbf{y}) & \text{if } \mathbf{y} \in \bar{\Gamma}_1 \\ f_2(\mathbf{y}) & \text{if } \mathbf{y} \in \bar{\Gamma}_2 \setminus \gamma, \end{cases} \quad (2.1)$$

where $\mathbf{y} = (y_1, \dots, y_N) \in \mathbb{R}^N$ and $f_1(\mathbf{y})$ and $f_2(\mathbf{y})$ are continuous functions in $\bar{\Gamma}_1$ and $\bar{\Gamma}_2 \setminus \gamma$, respectively. Based on the fact that $f(\mathbf{y}) = f_1(\mathbf{y})$ for $\mathbf{y} \in \gamma \subseteq \partial\Gamma_1$, we assume $f(\mathbf{y})$ has a jump discontinuity on γ such that

$$f_1(\mathbf{y}^*) = \lim_{\substack{\mathbf{y} \rightarrow \mathbf{y}^* \in \gamma \\ \mathbf{y} \in \Gamma_1}} f_1(\mathbf{y}) \neq \lim_{\substack{\mathbf{y} \rightarrow \mathbf{y}^* \in \gamma \\ \mathbf{y} \in \Gamma_2}} f_2(\mathbf{y}) < +\infty \quad \forall \mathbf{y}^* \in \gamma, \quad (2.2)$$

which means, without loss of generality, the discontinuity only occurs when approaching γ from the subdomain Γ_2 . The goal is to accurately capture the discontinuity hyper-surface γ . Again, without loss of generality, we also assume that $\partial\Gamma_1$ is a *continuous* hyper-surface such that Γ_1 and Γ_2 are disjoint. As such, there exists an *continuous* function $G(\mathbf{y}) = 0$ such that $\gamma = \{\mathbf{y} \in \bar{\Gamma} \mid G(\mathbf{y}) = 0\}$, i.e., γ is implicitly defined by the equation $G(\mathbf{y}) = 0$, and such that the target function f in (2.1) can

be expressed as

$$f(\mathbf{y}) = \begin{cases} f_1(\mathbf{y}) & \text{if } G(\mathbf{y}) \geq 0 \text{ for } \mathbf{y} \in \bar{\Gamma} \\ f_2(\mathbf{y}) & \text{if } G(\mathbf{y}) < 0 \text{ for } \mathbf{y} \in \bar{\Gamma}, \end{cases} \quad (2.3)$$

where $G(\mathbf{y}) > 0$ for $\mathbf{y} \in \bar{\Gamma}_1 \setminus \gamma$ and $G(\mathbf{y}) < 0$ for $\mathbf{y} \in \bar{\Gamma}_2 \setminus \gamma$. Note that $G(\mathbf{y}) = 0$ is only an abstract representation of γ and that its availability is not necessary for detecting the discontinuity. Moreover, for a specific γ , the $G(\mathbf{y})$ is not unique.

In one dimension, ($N = 1$), γ reduces to one or two points in $\Gamma \subset \mathbb{R}$ so that it is relatively easy to capture the discontinuity of $f(\mathbf{y})$. However, in higher dimensions ($N > 1$), detecting discontinuities becomes difficult because γ is, in general, an $N - 1$ dimensional hyper-surface with measure zero in \mathbb{R}^N . What is worse, there is no direct information available about the location or geometry of γ , so that we can only rely on indirect information about $f(\mathbf{y})$ and $G(\mathbf{y})$ to infer the location of γ . In this work, $f(\mathbf{y})$ in (2.3) is treated as a black-box function, i.e., given any $\mathbf{y} \in \bar{\Gamma}$ as an input, the function value can be obtained as an output without any knowledge about the analytical expressions of $f(\mathbf{y})$ or $G(\mathbf{y})$.

Before moving forward, we provide two examples of discontinuous functions of interest.

Example 2.1. Consider the generic function $f(\mathbf{y}) : \bar{\Gamma} \rightarrow \mathbb{R}$ defined in (2.3) with the implicit equation $G(\mathbf{y}) = 0$ given by

$$G(\mathbf{y}) = \mu^2 - \sum_{n=1}^N y_n^2 = 0,$$

where μ is a positive real constant such that $\gamma = \{\mathbf{y} \in \mathbb{R}^N \mid G(\mathbf{y}) = 0\} \subset \Gamma$. In this case, the discontinuity γ is a sphere in \mathbb{R}^N with radius μ and $\partial\Gamma_1 \cup \partial\Gamma = \emptyset$ and $\gamma = \partial\Gamma_1$. There are three specific scenarios one must consider:

- (S₁) $f(\mathbf{y})$ can be evaluated implicitly through, e.g., $f_1(\mathbf{y}) = \sin(y_1^2 + \cdots + y_N^2)$ and $f_2(\mathbf{y}) = \sin(y_1^2 + \cdots + y_N^2) + 0.5$;
- (S₂) $f(\mathbf{y})$ is the characteristic function of Γ_1 , e.g., $f_1(\mathbf{y}) = 1$ and $f_2(\mathbf{y}) = 0$;
- (S₃) Both $f(\mathbf{y})$ and $G(\mathbf{y})$ can be evaluated implicitly. \square

Example 2.2. [Probability of an event that depends on the the solution of an SPDE] Let D denote a bounded domain in \mathbb{R}^d , $d = 1, 2, 3$, and $(\Omega, \mathcal{F}, \mathbb{P})$ denote a complete probability space. Consider the following stochastic boundary value problem: find $u(\omega, \mathbf{x}) : \Omega \times \bar{D} \rightarrow \mathbb{R}^m$ such that \mathbb{P} -almost everywhere in Ω

$$\mathcal{L}(a)(u) = h \quad \text{in } D, \quad (2.4)$$

where the coefficient $a(\omega, \mathbf{x})$ of the differential operator \mathcal{L} and the right-hand side $h(\omega; \mathbf{x})$ are random fields. As in [3, 11, 12, 18], we assume the random fields a and h in (2.4) depend on a finite number of uncorrelated bounded random variables, i.e., on

an N -dimensional random vector $\mathbf{y}(\omega) = (y_1(\omega), \dots, y_N(\omega))$. We denote the image of y_n by $\Gamma_n = y_n(\Omega) \subset \mathbb{R}$ and define Γ as the interior of $\prod_{n=1}^N \Gamma_n$. By assuming that \mathbf{y} has a joint probability density function $\rho(\mathbf{y}): \bar{\Gamma} \rightarrow \mathbb{R}_+$ with $\rho(\mathbf{y}) \in L^\infty(\bar{\Gamma})$, the probability space $(\Omega, \mathcal{F}, \mathbb{P})$ is mapped to $(\bar{\Gamma}, \mathcal{B}(\bar{\Gamma}), \rho(\mathbf{y})d\mathbf{y})$, where $\mathcal{B}(\bar{\Gamma})$ denotes the Borel σ -algebra on $\bar{\Gamma}$ and $\rho(\mathbf{y})d\mathbf{y}$ the finite measure. According to the Doob-Dynkin lemma [13], the solution u can be expressed as $u(\mathbf{y}(\omega), \cdot) = u(y_1(\omega), \dots, y_N(\omega), \cdot)$.

In practice, we may be interested in quantifying the probability of an event that depends on $u(\mathbf{y}, \mathbf{x})$. For example, such a quantity of interest is the probability of the event that the spatial average $F(u) = \frac{1}{|D|} \int_D u(\mathbf{y}, \mathbf{x})d\mathbf{x}$ exceeds a threshold value \bar{u} , where $|D|$ denotes the volume of the spatial (physical) domain D . This probability can be expressed as

$$\mathbb{P}(F(u) \geq \bar{u}) = \int_{\bar{\Gamma}} \mathcal{X}_{\{F(u) \geq \bar{u}\}}(\mathbf{y})d\rho(\mathbf{y}), \quad (2.5)$$

where $\mathcal{X}_{\{F(u) \geq \bar{u}\}}(\mathbf{y})$ denotes the characteristic function of the event $\{F(u) \geq \bar{u}\}$. In this case, the target function $f(\mathbf{y})$ is the characteristic function $\mathcal{X}_{\{F(u) \geq \bar{u}\}}(\mathbf{y})$ and the discontinuity hyper-surface γ is determined by the implicit equation $G(\mathbf{y}) = F(u(\mathbf{y})) - \bar{u} = 0$. \square

From the above examples, we observe that, in practice, there may be additional indirect information available about $f(\mathbf{y})$ and $G(\mathbf{y})$ that can help one capture discontinuities. For instance, in Example 2.2, when defining $\Gamma_1 = \{\mathbf{y} \in \Gamma \mid \mathcal{X}_{\{F(u) \geq \bar{u}\}}(\mathbf{y}) = 1\}$, the function $G(\mathbf{y})$ can be evaluated as well and the membership of a given $\mathbf{y} \in \Gamma$ in the subdomain Γ_1 can be determined by the computable value of $f(\mathbf{y})$. Thus, in this paper, we consider discontinuity detection problems under one of the following three assumptions:

- A₁**: Given $\mathbf{y} \in \Gamma$, only $f(\mathbf{y})$ can be evaluated;
- A₂**: Given $\mathbf{y} \in \Gamma$, the value $f(\mathbf{y})$ can determine if $f(\mathbf{y}) = f_1(\mathbf{y})$ or $f(\mathbf{y}) = f_2(\mathbf{y})$, i.e., if $\mathbf{y} \in \Gamma_1$ or $\mathbf{y} \in \Gamma_2$;
- A₃**: Given $\mathbf{y} \in \Gamma$, both $f(\mathbf{y})$ and $G(\mathbf{y})$ can be evaluated.

It is easy to see that **A₂** is a sufficient condition for **A₁** and that **A₃** is a sufficient condition for both **A₁** and **A₂**. Under **A₁**, it is known that there exist jump discontinuities in Γ , but no information about the location of γ can be inferred from the function values of $f(\mathbf{y})$. In the context of **A₂**, function values of $f(\mathbf{y})$ can indicate the membership of a given point $\mathbf{y} \in \Gamma$ in the subdomain $\bar{\Gamma}_1 \in \Gamma$, which is referred to as the *characteristic property*. Under **A₃**, because $G(\mathbf{y})$ can be evaluated directly, detecting γ is equivalent to finding all the roots of the implicit equation $G(\mathbf{y}) = 0$. In one dimension ($N = 1$), this is straightforward to accomplish using classic root-finding algorithms, e.g., the bisection method. In higher dimensions, classic root-finding methods might make it easy to find one root but approximately

determining the whole surface γ is, in general, difficult. It is natural to look for more efficient algorithms for dealing with discontinuous functions satisfying \mathbf{A}_2 or \mathbf{A}_3 . Such improved methods are discussed in detail in §4.

Because it is almost impossible to solve for the analytical expression describing the hyper-surface γ , the main goal of our effort is to efficiently construct, in N dimensions, an accurate approximate hyper-surface, denoted by $\tilde{\gamma}$. To assess the performance of our approaches, the *accuracy* of $\tilde{\gamma}$ as an approximation of γ is measured by the distance between γ and $\tilde{\gamma}$ defined as

$$e_\infty = \text{dist}(\gamma, \tilde{\gamma}) = \max_{\mathbf{x} \in \gamma} \min_{\mathbf{x}' \in \tilde{\gamma}} |\mathbf{x}' - \mathbf{x}|. \quad (2.6)$$

In addition, as indicated in (2.5), we are also interested in estimating the integral of $f(\mathbf{y})$ over a subdomain of interest, i.e., either Γ_1 or Γ_2 . Without loss of generality, the *accuracy* of $\tilde{\gamma}$ is thus also assessed by the metric

$$e_{\text{int}} = \left| \int_{\Gamma_1} f(\mathbf{y}) d\mathbf{y} - \int_{\tilde{\Gamma}_1} f(\mathbf{y}) d\mathbf{y} \right|, \quad (2.7)$$

where $\tilde{\Gamma}_1$ is the approximation of Γ_1 resulting from the approximation $\tilde{\gamma}$ of γ . On the other hand, as shown in Example 2.2, the computational cost on evaluating $f(\mathbf{y})$ or $G(\mathbf{y})$ often dominates the total cost of constructing $\tilde{\gamma}$, e.g., because of the complexity of the PDE solver required to perform those evaluations. Thus, we use the number of function evaluations of either $f(\mathbf{y})$ or $G(\mathbf{y})$ as the metric to assess the *efficiency* of constructing $\tilde{\gamma}$.

As discussed in §1, a straightforward way to estimate the integral $\int_{\Gamma_1} f(\mathbf{y}) d\mathbf{y}$ is to use Monte Carlo methods, but the computational cost may not be affordable due to the slow convergence of such methods. Alternatively, the adaptive hierarchical sparse-grid (AHSG) method has been employed in discontinuity detection [8], but its efficiency deteriorates dramatically as the dimension N increases. The new approach proposed in §4 is a variant of the AHSG method but features much improved efficiency. To set the stage, before introducing our approach, we will briefly review, in §3, the standard AHSG method and illustrate its unsatisfactory performance in discontinuity detection settings.

3. Adaptive hierarchical sparse-grid approximation. In §3.1, we briefly review hierarchical sparse-grid interpolation that is the foundation of adaptive hierarchical sparse-grid (AHSG) interpolation. In §3.2, the AHSG method is introduced and its shortcomings in high-dimensional discontinuity detection is illustrated via a numerical example.

3.1. Hierarchical sparse-grid interpolation. The goal is to construct a Lagrange interpolant to a function $\eta(\mathbf{y}) : \Gamma \rightarrow \mathbb{R}$. Instead of using standard locally supported nodal piecewise polynomial bases, we build the interpolant using hierarchical piece-

wise polynomials [5].

We begin with the one-dimensional hat function having support $[-1, 1]$, given by $\psi(y) = \max\{0, 1 - |y|\}$. An arbitrary hat function with support $(y_{l,i} - h_l, y_{l,i} + h_l)$ can be generated by dilation and translation, i.e., $\psi_{l,i}(y) = \psi\left(\frac{y+1-ih_l}{h_l}\right)$, where l denotes the resolution level, $h_l = 2^{-l+1}$ for $l = 0, 1, \dots$ denotes the grid size of the level l grid, and $y_{l,i} = i h_l - 1$ for $i = 0, 1, \dots, 2^l$ denotes the grid points of the grid. The basis function $\psi_{l,i}(y)$ has local support with respect to the level l grid and is centered at the grid point $y_{l,i}$; the number of grid points in the level l grid is $2^l + 1$. With $V = L^2_\rho(\Gamma)$, a sequence of subspaces $\{V_l\}_{l=0}^\infty$ of V of increasing dimension $2^l + 1$ can be defined as

$$V_l = \text{span}\{\psi_{l,i}(y) \mid i = 0, 1, \dots, 2^l\} \quad \text{for } l \in \mathbb{N}.$$

The sequence is dense in V , i.e., $\cup_{l=0}^\infty V_l = V$, and nested, i.e., $V_0 \subset V_1 \subset \dots \subset V_l \subset V_{l+1} \subset \dots \subset V$. Each of the subspaces $\{V_l\}_{l=0}^\infty$ is the standard finite element subspace of continuous piecewise linear polynomial functions on $[-1, 1]$ that is defined with respect to the grid having mesh size h_l . The set $\{\psi_{l,i}(y)\}_{i=0}^{2^l}$ is the standard nodal basis for the space V_l .

An alternative to the nodal basis $\{\psi_{l,i}(y)\}_{i=0}^{2^l}$ for V_l is a *hierarchical* basis that we now construct, starting with the hierarchical index sets $B_l = \{i = 1, 3, 5, \dots, 2^l - 1\}$ for $l \in \mathbb{N}_+$ and the sequence of hierarchical subspaces defined by

$$W_l = \text{span}\{\psi_{l,i}(y) \mid i \in B_l\} \quad \text{for } l \in \mathbb{N}_+.$$

Due to the nesting property of $\{V_l\}_{l=0}^\infty$, we have that $V_l = V_{l-1} \oplus W_l$ and $W_l = V_l / \oplus_{l'=0}^{l-1} V_{l'}$ for $l \in \mathbb{N}_+$. We also have the hierarchical subspace splitting of V_l given by $V_l = V_0 \oplus W_1 \oplus \dots \oplus W_l$ for $l \in \mathbb{N}$.

For each grid level $l > 0$, the interpolant of a continuous function $\eta(y)$ in the subspace V_l in terms of the its nodal basis $\{\psi_{l,i}(y)\}_{i=0}^{2^l}$ is given by

$$\mathcal{U}_l(\eta) = \sum_{i=0}^{2^l} \eta(y_{l,i}) \cdot \psi_{l,i}(y). \quad (3.1)$$

Due to the nesting property $V_l = V_{l-1} \oplus W_l$, it is easy to see that $\mathcal{U}_{l-1}(\eta) = \mathcal{U}_l(\mathcal{U}_{l-1}(\eta))$, based on which we define the incremental interpolation operator

$$\Delta_l = \mathcal{U}_l - \mathcal{U}_{l-1} \quad \text{for } l \geq 0 \quad \text{with } \mathcal{U}_{-1} = 0. \quad (3.2)$$

Note that $\Delta_l(\eta)$ only involves the basis functions for W_l for $l \geq 1$. The interpolant $\mathcal{U}_l(\eta)$ for any level $l > 0$ can be then decomposed in the form

$$\mathcal{U}_l(\eta) = \mathcal{U}_{l-1}(\eta) + \Delta_l(\eta) = \dots = \mathcal{U}_0(\eta) + \sum_{l'=1}^l \Delta_{l'}(\eta). \quad (3.3)$$

Next we consider the hierarchical sparse-grid interpolation of a multivariate function $\eta(\mathbf{y})$ defined, again without loss of generality, over the unit hypercube $\Gamma = [-1, 1]^N \subset \mathbb{R}^N$. The one-dimensional hierarchical polynomial basis can be extended to the N -dimensional domain Γ using tensorization. Specifically, the N -variate basis function $\psi_{\mathbf{l},\mathbf{i}}(\mathbf{y})$ associated with the point $\mathbf{y}_{\mathbf{l},\mathbf{i}} = (y_{l_1,i_1}, \dots, y_{l_N,i_N})$ is defined using tensor products, i.e., $\psi_{\mathbf{l},\mathbf{i}}(\mathbf{y}) := \prod_{n=1}^N \psi_{l_n,i_n}(y_n)$, where $\mathbf{l} = (l_1, \dots, l_N)$ is a multi-index indicating the resolution level of the basis function. Note that the resolution level can be different in each of the N directions. The N -dimensional hierarchical incremental subspace $W_{\mathbf{l}}$ is defined by

$$W_{\mathbf{l}} = \bigotimes_{n=1}^N W_{l_n} = \text{span} \{ \psi_{\mathbf{l},\mathbf{i}}(\mathbf{y}) \mid \mathbf{i} \in B_{\mathbf{l}} \},$$

where the multi-index set $B_{\mathbf{l}}$ is given by

$$B_{\mathbf{l}} := \left\{ \mathbf{i} \in \mathbb{N}^N \mid \begin{array}{ll} i_n \in \{1, 3, 5, \dots, 2^{l_n} - 1\} & \text{for } n = 1, \dots, N \text{ if } l_n > 0 \\ i_n \in \{0, 1\} & \text{for } n = 1, \dots, N \text{ if } l_n = 0 \end{array} \right\}. \quad (3.4)$$

Then, a sequence of subspaces $\{\mathcal{V}_l\}_{l=0}^{\infty}$ of the space $\mathcal{V} = L^2_{\rho}(\Gamma)$ can be constructed using a sparse-grid framework, i.e.,

$$\mathcal{V}_l = \bigoplus_{l'=0}^l \mathcal{W}_{l'} = \bigoplus_{l'=0}^l \bigoplus_{|\mathbf{l}'|=l'} W_{l'}, \quad (3.5)$$

where $\mathbf{l} = (l_1, \dots, l_N) \in \mathbb{N}^N$ is a multi-index and $|\mathbf{l}| \equiv l_1 + \dots + l_N \leq l$ defines the resolution level of the sparse polynomial space \mathcal{V}_l . Note that full tensor-product space is defined by simply replacing the index set $|\mathbf{i}| \leq l$ by $\max\{i_1, \dots, i_N\} \leq l$ in (3.5). Similar to the one-dimensional case, $\{\mathcal{V}_l\}_{l=0}^{\infty}$ also has the nesting property such that $\mathcal{V}_l = \mathcal{V}_{l-1} \oplus \mathcal{W}_l$, where $\mathcal{W}_l = \mathcal{V}_l / \bigoplus_{l'=0}^{l-1} \mathcal{V}_{l'}$. We also have the hierarchical subspace splitting of \mathcal{V}_l given by $\mathcal{V}_l = \mathcal{V}_0 \oplus \mathcal{W}_1 \oplus \dots \oplus \mathcal{W}_l$. Then, the level L hierarchical sparse-grid approximation $\eta_L(\mathbf{y}) \in \mathcal{V}_L$ of the target function $\eta(\mathbf{y})$ is defined by

$$\begin{aligned} \eta_L(\mathbf{y}) &= \sum_{l=0}^L \sum_{|\mathbf{l}|=l} (\Delta_{l_1} \otimes \dots \otimes \Delta_{l_N})(\eta)(\mathbf{y}) \\ &= \eta_{L-1}(\mathbf{y}) + \sum_{|\mathbf{l}|=L} (\Delta_{l_1} \otimes \dots \otimes \Delta_{l_N})(\eta)(\mathbf{y}) \\ &= \eta_{L-1}(\mathbf{y}) + \sum_{|\mathbf{l}|=L} \sum_{\mathbf{i} \in B_{\mathbf{l}}} [\eta(\mathbf{y}_{\mathbf{l},\mathbf{i}}) - \eta_{L-1}(\mathbf{y}_{\mathbf{l},\mathbf{i}})] \psi_{\mathbf{l},\mathbf{i}}(\mathbf{y}), \\ &= \eta_{L-1}(\mathbf{y}) + \sum_{|\mathbf{l}|=L} \sum_{\mathbf{i} \in B_{\mathbf{l}}} \omega_{\mathbf{l},\mathbf{i}} \psi_{\mathbf{l},\mathbf{i}}(\mathbf{y}), \end{aligned} \quad (3.6)$$

where $\omega_{\mathbf{l},\mathbf{i}} = \eta(\mathbf{y}_{\mathbf{l},\mathbf{i}}) - \eta_{L-1}(\mathbf{y}_{\mathbf{l},\mathbf{i}})$ denotes the *multi-dimensional hierarchical surplus*. This interpolant is a direct extension, via the Smolyak algorithm, of the one-dimensional hierarchical interpolant. The definition of the surplus $w_{\mathbf{l},\mathbf{i}}$ is based on the facts that $\eta_l(\eta_{l-1}(\mathbf{y})) = \eta_{l-1}(\mathbf{y})$ and $\eta_{l-1}(\mathbf{y}_{\mathbf{l},\mathbf{i}}) - \eta(\mathbf{y}_{\mathbf{l},\mathbf{i}}) = 0$ for $|\mathbf{l}| = l$.

We denote by $\mathcal{H}_1(\Gamma) = \{\mathbf{y}_{\mathbf{l},\mathbf{i}} \mid \mathbf{i} \in B_1\}$ the set of points corresponding to the subspace W_1 . Then, the set of points corresponding to the subspace \mathcal{W}_l is given by $\bigcup_{|\mathbf{l}|=l} \mathcal{H}_1(\Gamma)$, and the sparse grid corresponding to the interpolant η_L is given by

$$\mathcal{H}_L(\Gamma) = \bigcup_{|\mathbf{l}| \leq L} \mathcal{H}_1(\Gamma),$$

where $\mathcal{H}_l(\Gamma)$ is also nested, i.e., $\mathcal{H}_{l-1}(\Gamma) \subset \mathcal{H}_l(\Gamma)$. In addition, with $\Delta\mathcal{H}_0(\Gamma) = \mathcal{H}_0(\Gamma)$, we denote by $\Delta\mathcal{H}_l(\Gamma) = \mathcal{H}_l(\Gamma) \setminus \mathcal{H}_{l-1}(\Gamma)$ the set of newly added sparse grid points on level l .

3.2. Adaptive hierarchical sparse-grid interpolation. By virtue of the hierarchical surpluses $\omega_{\mathbf{l},\mathbf{i}}$, the interpolant in (3.6) can be represented in a hierarchical manner, i.e.,

$$\eta_L(\mathbf{y}) = \eta_{L-1}(\mathbf{y}) + \Delta\eta_L(\mathbf{y}),$$

where $\eta_{L-1}(\mathbf{y})$ is the sparse-grid interpolant in \mathcal{V}_{L-1} and $\Delta\eta_L(\mathbf{y})$ is the hierarchical surplus interpolant in the subspace \mathcal{W}_L . According to the analysis in [5], for smooth functions, the surpluses $\omega_{\mathbf{l},\mathbf{i}}$ of the sparse-grid interpolant $\eta_L(\mathbf{y})$ tend to zero as the resolution level L tends to infinity. For example, in the context of using piecewise-linear hierarchical bases and $\eta(\mathbf{y})$ having bounded second-order weak derivatives with respect to \mathbf{y} , the surplus $\omega_{\mathbf{l},\mathbf{i}}$ can be bounded as

$$|\omega_{\mathbf{l},\mathbf{i}}| \leq C_{\text{surp}} 2^{-2 \cdot |\mathbf{l}|} \quad \text{for } \mathbf{i} \in B_1, \quad (3.7)$$

where the constant C_{surp} is independent of the level $|\mathbf{l}|$. Furthermore, the smoother the target function is, the faster the surplus decays. This provides a good avenue for constructing adaptive sparse-grid interpolants using the magnitude of the surplus as an error indicator, especially for irregular functions having, e.g., steep slopes or jump discontinuities. Another adaptive sparse-grid approach using wavelet coefficients to guide mesh refinement is described in [6].

We first focus on the construction of one-dimensional adaptive grids and then extend the adaptivity process to multi-dimensional sparse grids. As shown in Figure 1, the one-dimensional hierarchical grid points have a tree-like structure. In general, a grid point $y_{l,i}$ on level l has two children on level $l+1$, namely $y_{l+1,2i-1}$ and $y_{l+1,2i+1}$. Special treatment is required when moving from level 0 to level 1, where we only add a single child $y_{1,1}$. At each successive interpolation level, the basic idea of adaptivity is to use the hierarchical surplus as an error indicator to detect the smoothness of the target function and refine the grid by adding two new points on the next level for each point for which the magnitude of the surplus is larger than the prescribed

error tolerance. For example, in Figure 1, we illustrate the 6-level adaptive grid for interpolating the function $\eta(y) = \exp[-(y - 0.4)^2/0.0625^2]$ on $[0, 1]$ with error tolerance 0.01. Because the magnitude of every surplus is larger than 0.01 for all points in levels 0, 1, and 2, as mentioned above, one point is added to the level 0 points and 2 points are added at levels 1 and 2. This takes us to level 3 where we find that only 1 point, namely $y_{3,3}$, has a surplus whose magnitude is larger than 0.01, so only two new points are added on level 4. If we continue through levels 5 and 6, we end up with the 6-level adaptive grid with only 21 points (points in black in Figure 1), whereas the 6-level non-adaptive grid has a total of 65 points (points in black and gray in Figure 1).

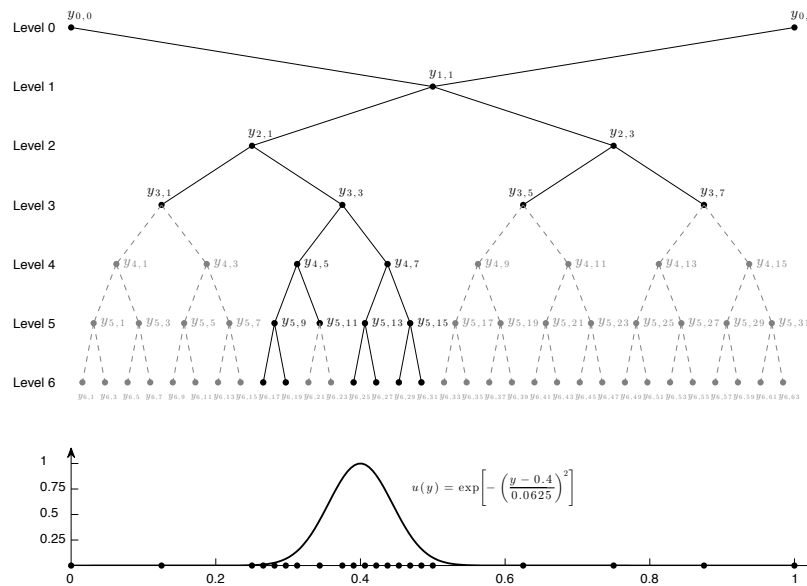


Figure 1: A 6-level adaptive sparse grid for interpolating the one-dimensional function $\eta(y) = \exp[-(y - 0.4)^2/0.0625^2]$ on $[0, 1]$ picture on the bottom plot with an error tolerance of 0.01. The resulting adaptive sparse grid has only 21 points (black points) whereas the full grid has 65 points (black and gray points).

It is a trivial matter to extend the adaptivity from the one-dimension to the multi-dimensional adaptive sparse grid. In general, a grid point in a N -dimensional space has $2N$ children which are also the neighbor points of the parent node. We start with an isotropic sparse grid of level L_{\min} and build an approximation $\eta_{L_{\min}}(\mathbf{y})$ in order to capture the main profile of the target function. Note that the children of a parent point correspond to hierarchical basis functions on the next interpolation level. Thus, for $L \geq L_{\min}$, we only add those grid points on level L whose parent on level $L - 1$ has a surplus greater than the prescribed tolerance. In this way, the sparse grid can be refined locally and we end up with an adaptive sparse grid which is a sub-grid of the corresponding isotropic sparse grid.

However, according to the analysis in [5], such a mesh refinement strategy will not stop automatically if the target function has jump discontinuities because the surplus will not decay to zero around the discontinuities. To mandate the termination of the refinement iteration, one has to set a maximum allowable resolution level L_{\max} , i.e., one stops refining the sparse grid when $L = L_{\max}$. Hence, the N -dimensional adaptive sparse-grid interpolant of level L with the error tolerance being $\alpha > 0$ can be represented by

$$\eta_{L,\alpha}(\mathbf{y}) = \sum_{l=0}^L \sum_{|\mathbf{l}|=l} \sum_{\mathbf{i} \in B_1^\alpha} \omega_{\mathbf{l},\mathbf{i}} \psi_{\mathbf{l},\mathbf{i}}(\mathbf{y}), \quad (3.8)$$

where $L \leq L_{\max}$ and the multi-index set $B_1^\alpha \subseteq B_1$ is defined by $B_1^\alpha = \{\mathbf{i} \in B_1 \mid |\omega_{\mathbf{l},\mathbf{i}}| \geq \alpha\}$. Note that $B_1^\alpha = B_1$ for $|\mathbf{l}| \leq L_{\min}$; for $L_{\min} < L \leq L_{\max}$, B_1^α is an optimal multi-index set that contains only the indices of the basis functions corresponding to surplus magnitudes larger than the tolerance α . However, in practice, the function $\eta(\mathbf{y})$ needs to be evaluated at a certain number of grid points $\mathbf{y}_{\mathbf{l},\mathbf{i}}$ with $|\omega_{\mathbf{l},\mathbf{i}}| \leq \alpha$ in order to detect when mesh refinement can stop. The corresponding adaptive sparse grid is represented by $\mathcal{H}_{L,\alpha}(\Gamma) = \bigcup_{l=0}^L \Delta \mathcal{H}_{l,\alpha}(\Gamma)$, where $\Delta \mathcal{H}_{l,\alpha}(\Gamma) = \Delta \mathcal{H}_l(\Gamma)$ for $l = 0, \dots, L_{\min}$, and $\Delta \mathcal{H}_{l,\alpha}(\Gamma)$ for $l = L_{\min} + 1, \dots, L_{\max}$, only contains the sparse grid points added by the mesh refinement. Note that if the target function is continuous or smoother, the mesh refinement may stop at a level L smaller than the maximum allowable level L_{\max} .

In the literature, the AHS method has been used to approximate irregular functions [5, 10], e.g., having steep slopes, sharp transitions, or jump discontinuities, in low dimensional spaces ($N \leq 3$). However, in these cases, the AHS method cannot achieve the desired efficiency as in approximating smooth functions. What is worse, the AHS approach will eventually converge slower than a simple Monte Carlo method, even for a moderate 4-dimensional discontinuous function, as shown in the following example.

Example 3.1. *The target $f(\mathbf{y})$ is the characteristic function in \mathbb{R}^N given by*

$$f(\mathbf{y}) = \begin{cases} 1 & \text{if } 1 - y_1^2 - \dots - y_N^2 \geq 0, \\ 0 & \text{otherwise,} \end{cases} \quad (3.9)$$

where the discontinuity hyper-surface γ is the unit hyper-sphere in \mathbb{R}^N . For $N = 1, 2, 3, 4$, $L_{\min} = 4$, and $L_{\max} = 100$, we build AHS approximation $f_{L,\alpha}(\mathbf{y})$ with $\alpha = 0.01$. The error is measured by the metric e_{int} defined in (2.7). Because the surplus will not decay to zero around the hyper-sphere, mesh refinement will not stop until the level L reaches L_{\max} . Thus, we compute and plot, in Figure 2, of the error e_{int} vs. the number of function evaluations, by increasing the resolution level L up to L_{\max} . For comparison, the error of Monte Carlo simulations are also plotted in Figure 2. We observe that the AHS approximation outperforms Monte Carlo in the one and two-dimensions, but performs similarly in three dimensions, and, in four

dimensions, Monte Carlo outperforms AHSG.

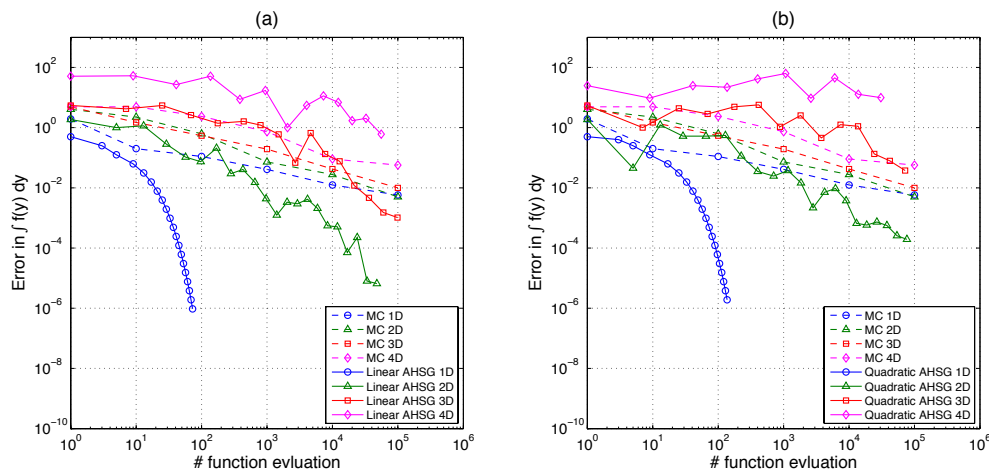


Figure 2: The error in the approximations of the integral of $f(\mathbf{y})$ given by (3.9) vs. the number of function evaluations, using the AHSG and Monte Carlo methods with $N = 1, 2, 3, 4$ for (a) the AHSG approximations with a piecewise-linear hierarchical basis and (b) the AHSG approximations with a piecewise-quadratic hierarchical basis.

To investigate the reason of such failures, we plot, in Figure 3, the resulting adaptive sparse grids in the two and three dimensions for an error $e_{int} < 0.01$. Note that mesh refinement places a dense set of grid points in the vicinity of the discontinuities, resulting in a loss of the desired grid sparsity. In fact, the N -dimensional hypersphere γ , across which the function is discontinuous, is approximated by an extremely dense grid. It is the loss of the sparsity that makes the AHSG approximation fail when attempting discontinuity detection in high-dimensional space. Moreover, because the target function $f(\mathbf{y})$ is discontinuous, the accuracy of the AHSG approximation cannot be improved by using high-order hierarchical basis [5]. In fact, the accuracy is worse for piecewise-quadratic approximations than it is for piecewise-linear approximations; see Figure 2.

4. Hyper-spherical adaptive sparse-grid method for discontinuity detection.

In this section, we propose a hyper-spherical adaptive hierarchical sparse-grid (HS-AHSG) method that overcomes the disadvantages of the AHSG method for high-dimensional discontinuity detection. The basic idea is to directly approximate the discontinuity hyper-surface γ itself, instead of refining the sparse grid in its vicinity, i.e., instead of refining in a neighborhood of γ having non-zero volume in \mathbb{R}^N . Unlike the discontinuous function $f(\mathbf{y})$ in (2.3), the hyper-surface γ is usually smooth, so that the drawbacks of the AHSG method mentioned above can be avoided when directly approximating γ . However, in general, the hyper-surface γ is not a function in the Cartesian coordinate system in \mathbb{R}^N , so that the hyper-spherical transformation is introduced into our approach to convert γ into a function in the hyper-spherical

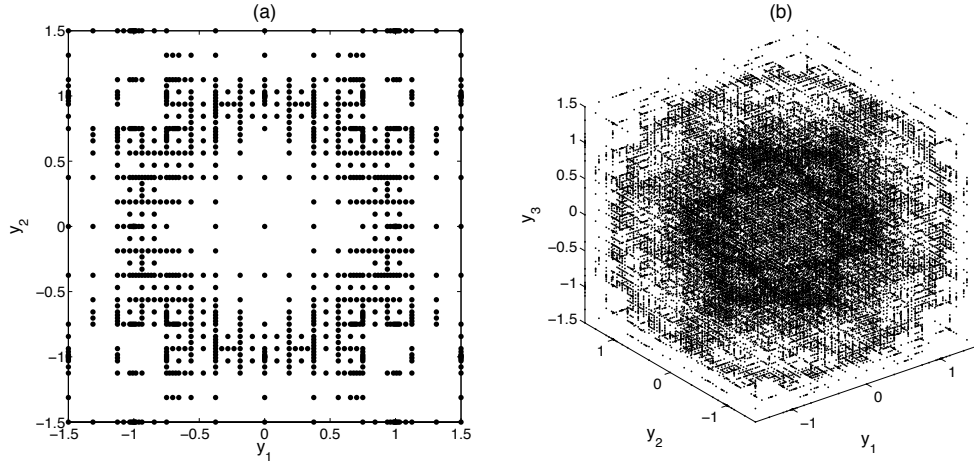


Figure 3: The grids produced by the AHSG method for approximating the integral of $f(\mathbf{y})$ given by (3.9) with linear hierarchical basis and $e_{\text{int}} < 0.01$: (a) the two-dimensional sparse grid has 969 points; (b) the three-dimensional sparse grid has 936,093 points.

coordinate system. Details about the conversion and the evaluation of the transformed function are discussed in §4.1 and §4.2, respectively. The main HS-AHSG algorithm is described in §4.3. In §4.4, the efficiency of the proposed algorithm is improved by incorporating the hierarchal acceleration technique proposed in [7]. Rigorous error estimate and ε -complexity analyses are provided in §4.5, for the algorithms discussed in §4.3 and §4.4.

4.1. Representation of the discontinuity surface in the hyper-spherical coordinate system. A hyper-spherical coordinate system is a generalization of the two-dimensional polar and three-dimensional spherical coordinate systems. It has: one radial coordinate r ranging over $[0, \infty)$; one angular coordinate θ_{N-1} ranging over $[0, 2\pi)$ and; $N - 2$ angular coordinates $\theta_1, \dots, \theta_{N-2}$ ranging over $[0, \pi)$. Denoting by $\Gamma_s = [0, \pi)^{N-2} \times [0, 2\pi)$, the relation between the hyper-spherical coordinates $(r, \theta_1, \dots, \theta_{N-1}) \in [0, \infty) \times \Gamma_s$ and the Cartesian coordinates $\mathbf{y} = (y_1, \dots, y_N) \in \mathbb{R}^N$ is given by

$$\begin{cases} y_1 = y_{0,1} + r \cos(\theta_1) \\ y_2 = y_{0,2} + r \sin(\theta_1) \cos(\theta_2) \\ y_3 = y_{0,3} + r \sin(\theta_1) \sin(\theta_2) \cos(\theta_3) \\ \vdots \\ y_{N-1} = y_{0,N-1} + r \sin(\theta_1) \cdots \sin(\theta_{N-2}) \cos(\theta_{N-1}) \\ y_N = y_{0,N} + r \sin(\theta_1) \cdots \sin(\theta_{N-2}) \sin(\theta_{N-1}), \end{cases} \quad (4.1)$$

where $\mathbf{y}_0 = (y_{0,1}, \dots, y_{0,N})$ denotes the origin of the hyper-spherical coordinate system. Based on this transformation, we would like to transform the discontinu-

ity hyper-surface γ defined by the *implicit* equation $G(\mathbf{y}) = 0$ in (2.3) into the hyper-spherical coordinate system, and represent it by an *explicit* function of $\boldsymbol{\theta} = (\theta_1, \dots, \theta_{N-1})$. To achieve this, we make the following assumption on the geometry of the subdomain Γ_1 and the origin \mathbf{y}_0 .

Assumption 4.1. *For the underlying domain $\Gamma = \Gamma_1 \cup \gamma \cup \Gamma_2$ in (2.1), we assume that Γ_1 is a star-convex domain in \mathbb{R}^N and that a point \mathbf{y}_0 in Γ_1 is given such that, for all $\mathbf{y} \in \Gamma_1$, the line segment $\{\mathbf{y}_0 + t\mathbf{y} \mid t \in [0, 1]\}$ from \mathbf{y}_0 to \mathbf{y} is in Γ_1 .*

Remark 4.2. When Γ_1 is a convex domain, it is also star-convex and any point in Γ_1 can be used as the origin \mathbf{y}_0 ; the function given in Example 2.1 provides an example of this case. If \mathbf{y}_0 is not known a priori, it can be obtained by Monte Carlo sampling in Γ , as long as $f(\mathbf{y})$ has the characteristic property. In practice, \mathbf{y}_0 is sometimes available for the problem of interest. For instance, as discussed in Example 2.2, the interest of investigating the probability of an event usually results from the occurrence of such event in a physical experiment with a specific set of parameter values. In this case, these values can be used to define the origin \mathbf{y}_0 . On the other hand, if Γ_1 is not convex, the set of points qualified to be used as \mathbf{y}_0 is only a subset of Γ_1 . In this case, especially when the target function has no characteristic property, it is much more difficult to choose a qualified \mathbf{y}_0 .

Based on the transformation (4.1) with origin \mathbf{y}_0 satisfying Assumption 4.1, there exists a unique $N - 1$ dimensional continuous function $g(\boldsymbol{\theta}) : \Gamma_s \rightarrow [0, \infty)$ such that $\partial\Gamma_1 = \{(g(\boldsymbol{\theta}), \boldsymbol{\theta}) \mid \forall \boldsymbol{\theta} \in \Gamma_s\}$. The value of $g(\boldsymbol{\theta})$ is the Euclidean distance between the origin \mathbf{y}_0 and $\partial\Gamma_1$ along the direction $\boldsymbol{\theta}$. Under the definitions in §2, given $\boldsymbol{\theta} \in \Gamma_s$, there are two possibilities for the location of $(g(\boldsymbol{\theta}), \boldsymbol{\theta})$, i.e., $(g(\boldsymbol{\theta}), \boldsymbol{\theta}) \in \partial\Gamma \cup \partial\Gamma_1$ or $(g(\boldsymbol{\theta}), \boldsymbol{\theta}) \in \gamma \subseteq \partial\Gamma_1$. Thus, $g(\boldsymbol{\theta})$ is the desired function representation of the discontinuity hyper-surface γ . Unlike the *implicit* equation $G(\mathbf{y}) = 0$, $g(\boldsymbol{\theta})$ is an *explicit* representation of γ , so that it becomes feasible to estimate γ directly by approximating $g(\boldsymbol{\theta})$ in the bounded domain Γ_s . However, Assumption 4.1 only guarantees the existence of $g(\boldsymbol{\theta})$ and the value of $g(\boldsymbol{\theta})$ at $\boldsymbol{\theta} \in \Gamma_s$ is unknown a priori. Therefore, a strategy of evaluating $g(\boldsymbol{\theta})$ is provided in §4.2.

Before moving forward, for clarity, in Table 1 we list and explain the notations used in the sequel.

4.2. Evaluation of the function representation of γ . We now investigate how the transformed function $g(\boldsymbol{\theta})$ of the discontinuity hyper-surface γ can be evaluated at a given point $\boldsymbol{\theta} \in \Gamma_s$. Essentially, taking advantage of the hyper-spherical transformation, the evaluation of $g(\boldsymbol{\theta})$ becomes a discontinuity detection problem for a one-dimensional function $f_{\boldsymbol{\theta}}(r)$ in the interval $[S_r(\mathbf{y}_0), S_r(\boldsymbol{\beta}_{\boldsymbol{\theta}})]$. If $(g(\boldsymbol{\theta}), \boldsymbol{\theta}) \in \partial\Gamma \cap \partial\Gamma_1$, then $f_{\boldsymbol{\theta}}(r)$ is a continuous function on the line segment $\{\mathbf{y}_0 + t\boldsymbol{\beta}_{\boldsymbol{\theta}} \mid t \in [0, 1]\}$, such that $g(\boldsymbol{\theta}) = |\boldsymbol{\beta}_{\boldsymbol{\theta}} - \mathbf{y}_0|$; if $(g(\boldsymbol{\theta}), \boldsymbol{\theta}) \in \gamma \subset \partial\Gamma_1 \setminus \partial\Gamma$, then $f_{\boldsymbol{\theta}}(r)$ is discontinuous at $r = g(\boldsymbol{\theta})$ so that $g(\boldsymbol{\theta})$ can be estimated by capturing the discontinuity of $f_{\boldsymbol{\theta}}(r)$. Under Assumption **A**₁ given in §2, we cannot distinguish in advance whether $f_{\boldsymbol{\theta}}(r)$ is continuous or discontinuous in $[S_r(\mathbf{y}_0), S_r(\boldsymbol{\beta}_{\boldsymbol{\theta}})]$, so that one needs to first approximate the whole profile of $f_{\boldsymbol{\theta}}(r)$, then identify the existence and location of the discontinuity.

Table 1: Definition of notations

Notation	Explanation
$g(\boldsymbol{\theta})$	the function representation of $\partial\Gamma_1$ in $\Gamma_s = [0, \pi)^{N-2} \times [0, 2\pi)$
$\tilde{g}(\boldsymbol{\theta})$	the approximation of $g(\boldsymbol{\theta})$
$S(\mathbf{y})$	the transformation from Cartesian coordinates \mathbf{y} to hyper-spherical coordinates $(r, \boldsymbol{\theta})$
$S^{-1}(\mathbf{y})$	the inverse transformation of $S(\mathbf{y})$
$S_r(\mathbf{y})$	the transformation from \mathbf{y} to the radial coordinate r
$S_\theta(\mathbf{y})$	the transformation from \mathbf{y} to the angular coordinates $\boldsymbol{\theta} = (\theta_1, \dots, \theta_{N-1})$
$\boldsymbol{\beta}_\theta$	the Cartesian coordinates $(\beta_{\theta,1}, \dots, \beta_{\theta,N})$ of the intersection point of $\partial\Gamma \cap \partial\Gamma_1$ and the ray from \mathbf{y}_0 along the direction $\boldsymbol{\theta}$
$f_\theta(r)$	the target function f restricted to the ray along the direction $\boldsymbol{\theta}$, i.e., $f_\theta(r) = f(S^{-1}(r, \boldsymbol{\theta}))$

ity by analyzing the approximation. However, in the context of \mathbf{A}_2 or \mathbf{A}_3 , relying on the characteristic property, root-finding approaches can be employed to improve the efficiency of searching. We discuss the evaluation of $f(\mathbf{y})$ in the absence of the characteristic property in §4.2.1 and with the characteristic property in §4.2.2.

4.2.1. $f(\mathbf{y})$ without the characteristic property. Under Assumption \mathbf{A}_1 , $f(\mathbf{y})$ can be evaluated at a given point $\mathbf{y} \in \Gamma$, but one cannot determine whether or not the point \mathbf{y} is in $\Gamma_1 \cup \gamma$ from the value of $f(\mathbf{y})$. For each $\boldsymbol{\theta}$, because $f_\theta(r)$ is a one-dimensional function of r , we use the one-dimensional ASGH method to construct an adaptive approximation of $f_\theta(r)$ in the interval $[S_r(\mathbf{y}_0), S_r(\boldsymbol{\beta}_\theta)]$. As shown in Figure 1, the adaptivity will automatically refine in the region where $f_\theta(r)$ has large variations, including jump discontinuities. To find a value $\tilde{g}(\boldsymbol{\theta})$ such that $|\tilde{g}(\boldsymbol{\theta}) - g(\boldsymbol{\theta})| \leq \tau$, an adaptive interpolant is constructed by setting $\eta = f_\theta$ in (3.8), with the maximum level of the adaptive grid being $L_{\max} = \lceil \log_2(|\mathbf{y}_0 - \boldsymbol{\beta}_\theta|/\tau) \rceil$. Note that the hierarchical surplus decays to zero as the level L increases in the smooth region of $f_\theta(r)$, but not near the jump discontinuity. Thus, if the mesh refinement stops automatically at a level $L < L_{\max}$, it means that $f_\theta(r)$ is continuous in $[S_r(\mathbf{y}_0), S_r(\boldsymbol{\beta}_\theta)]$ so that $g(\boldsymbol{\theta}) = |\boldsymbol{\beta}_\theta - \mathbf{y}_0|$ and $(g(\boldsymbol{\theta}), \boldsymbol{\theta}) \in \partial\Gamma \cup \partial\Gamma_1$. Otherwise, due to Assumption 4.1, $f_\theta(r)$

has only one jump discontinuity at $(g(\boldsymbol{\theta}), \boldsymbol{\theta})$ and thus $\tilde{g}(\boldsymbol{\theta})$ can be determined by

$$(r_1, r_2) = \arg \max_{r, r' \in \mathcal{H}_{L_{\max}}([S_r(\mathbf{y}_0), S_r(\boldsymbol{\beta}_\theta)])} \frac{|f_\theta(r) - f_\theta(r')|}{|r - r'|} \quad \text{and} \quad \tilde{g}(\boldsymbol{\theta}) = \frac{1}{2}(r_1 + r_2),$$

where $[r_1, r_2]$ is the interval which contains the largest variation of $f_\theta(r)$ based on the available samples in $\mathcal{H}_{L_{\max}}([S_r(\mathbf{y}_0), S_r(\boldsymbol{\beta}_\theta)])$. If τ is sufficiently small, then we have $g(\boldsymbol{\theta}) \in [r_1, r_2]$ with $|r_1 - r_2| < \tau$.

4.2.2. $f(\mathbf{y})$ with characteristic property. Under Assumptions \mathbf{A}_2 or \mathbf{A}_3 , because the function value of $f(\mathbf{y})$ does decide on the membership of a given point $\mathbf{y} \in \Gamma$ in the subdomain $\Gamma_1 \cup \gamma \in \Gamma$, we can take advantage of such information to infer the existence or the location of the jump discontinuity of $f_\theta(r)$ for any $\boldsymbol{\theta} \in \Gamma_s$. Specifically, to evaluate $g(\boldsymbol{\theta})$ at $\boldsymbol{\theta} \in \Gamma_s$, we first evaluate $f(\mathbf{y})$ at $\mathbf{y} = \boldsymbol{\beta}_\theta$. If $f(\boldsymbol{\beta}_\theta) = f_1(\boldsymbol{\beta}_\theta)$, then $(g(\boldsymbol{\theta}), \boldsymbol{\theta}) \in \partial\Gamma \cap \partial\Gamma_1$ and $|\boldsymbol{\beta}_\theta - \mathbf{y}_0|$ is the exact value of $g(\boldsymbol{\theta})$. Otherwise, we have $(g(\boldsymbol{\theta}), \boldsymbol{\theta}) \in \gamma \subset \partial\Gamma_1$ and $g(\boldsymbol{\theta})$ is the location of the jump discontinuity of the function $f_\theta(r)$ which can be represented by

$$f_\theta(r) = \begin{cases} f_1(S^{-1}(r, \boldsymbol{\theta})) & \text{if } r \leq g(\boldsymbol{\theta}) \\ f_2(S^{-1}(r, \boldsymbol{\theta})) & \text{if } r > g(\boldsymbol{\theta}), \end{cases}$$

where $S^{-1}(r, \boldsymbol{\theta}) \in \Gamma$. Due to the characteristic property, several root-finding approaches can be applied to estimate the discontinuity of $f_\theta(r)$. The simplest choice is the bisection method. We start with $r_{-1} = 0$ and $r_0 = |\boldsymbol{\beta}_\theta - \mathbf{y}_0|$, where $f_\theta(r_{-1}) = f_1(S^{-1}(r_{-1}, \boldsymbol{\theta}))$ and $f_\theta(r_0) = f_2(S^{-1}(r_0, \boldsymbol{\theta}))$. In the k -th iteration, we have $r_k = (r_{k-1} + r_{k-2})/2$, where $f_\theta(r_{k-1}) = f_1(S^{-1}(r_{k-1}, \boldsymbol{\theta}))$ and $f_\theta(r_{k-2}) = f_2(S^{-1}(r_{k-2}, \boldsymbol{\theta}))$. For a prescribed accuracy τ such that $|\tilde{g}(\boldsymbol{\theta}) - g(\boldsymbol{\theta})| \leq \tau$, the necessary number of iterations K is given by

$$K = \left\lceil \log_2 (|\mathbf{y}_0 - \boldsymbol{\beta}_\theta| / \tau) \right\rceil \quad (4.2)$$

and the approximation is defined by $\tilde{g}(\boldsymbol{\theta}) = (r_K + r_{K-1})/2$. Note that the number of iterations K needed for bisection is the same as the maximum level L_{\max} needed for the one-dimensional AHSG method. Both methods have grids of the same minimum resolution for $L_{\max} = K$, but the bisection method requires fewer number of function evaluations because it only add one neighboring point at each iteration whereas the AHSG method adds two neighboring points at a time. Thus, the bisection method is preferable when $f(\mathbf{y})$ has the characterization property.

In case $f(\mathbf{y})$ satisfies Assumption \mathbf{A}_3 , i.e., the function $G(\mathbf{y})$ in (2.3) can be evaluated, other root-finding methods with faster convergence rates can be used to improve the efficiency of the search along the direction of $\boldsymbol{\theta} \in \Gamma_s$. For instance, the target function in Example (2.2) is a characteristic function and $G(\mathbf{y}) = \bar{u} - F(u(\mathbf{y}))$ can be evaluated for each $\mathbf{y} \in \Gamma$. The discontinuity of $f_\theta(r)$ can also be detected by searching the root of $G(S^{-1}(r, \boldsymbol{\theta})) = \bar{u} - F(u(S^{-1}(r, \boldsymbol{\theta}))) = 0$. If $G(\mathbf{y})$ is smooth

with respect to r , Newton's method or the secant methods can be used to achieve the desired accuracy with fewer iterations compared to the bisection method. In this work, we use the Regula Falsi method [14], a variant of the secant method. As is the case of using the bisection method, we start with $r_{-1} = 0$ and $r_0 = |\boldsymbol{\beta}_\theta - \mathbf{y}_0|$, where $G(S^{-1}(r_{-1}, \boldsymbol{\theta})) \geq 0$ and $G(S^{-1}(r_0, \boldsymbol{\theta})) < 0$. In the $k + 1$ -th iteration, r_{k+1} is defined by

$$r_{k+1} = r_k - G(S^{-1}(r_k, \boldsymbol{\theta})) \cdot \frac{r_k - r_{k'}}{G(S^{-1}(r_k, \boldsymbol{\theta})) - G(S^{-1}(r_{k'}, \boldsymbol{\theta}))}, \quad (4.3)$$

where k' is the maximum index less than k such that $G(S^{-1}(r_k, \boldsymbol{\theta})) \cdot G(S^{-1}(r_{k'}, \boldsymbol{\theta})) < 0$. It is known that the Regula Falsi method converges slower than the secant method but the iterates generated by (4.3) are all contained within the initial interval $[S_r(\mathbf{y}_0), S_r(\boldsymbol{\beta}_\theta)]$. Thus, one does not need to worry about the issue of getting negative r_k from (4.3). When $|r_k - r_{k'}|$ becomes sufficiently small, one can switch to the secant method to obtain faster convergence.

4.3. The hyper-spherical adaptive hierarchical sparse-grid algorithm. We now describe a complete procedure for the HS-AHSG method. Under Assumption 4.1, the hyper-surface γ can be represented by the transformed function $g(\boldsymbol{\theta})$ and we would like to build an adaptive sparse-grid interpolant of $g(\boldsymbol{\theta})$ in the $N - 1$ dimensional domain Γ_s . At each grid point $\boldsymbol{\theta}_{1,i}$, $g(\boldsymbol{\theta}_{1,i})$ is estimated by $\tilde{g}(\boldsymbol{\theta}_{1,i})$ using the approaches discussed in §4.2. Thus, we actually construct an interpolant of the approximation $\tilde{g}(\boldsymbol{\theta})$. As discussed in §3.2, for fixed L_{\min} , L_{\max} , and α , the adaptive sparse-grid interpolant at level L ($L_{\min} \leq L \leq L_{\max}$) is defined by setting $\eta(\boldsymbol{\theta}) = \tilde{g}(\boldsymbol{\theta})$ in (3.8), i.e.,

$$\tilde{g}_{L,\alpha}(\boldsymbol{\theta}) = \sum_{l=0}^L \sum_{|\mathbf{l}|=l} \sum_{\mathbf{i} \in B_1^\alpha} \tilde{\omega}_{1,\mathbf{i}} \cdot \psi_{1,\mathbf{i}}(\boldsymbol{\theta}), \quad (4.4)$$

where the surpluses $\{\tilde{\omega}_{1,\mathbf{i}} \mid |\mathbf{l}| \leq L, \mathbf{i} \in B_1^\alpha\}$ are computed based on the set of approximate function values

$$\{\tilde{g}(\boldsymbol{\theta}_{1,i}) \mid \boldsymbol{\theta}_{1,i} \in \mathcal{H}_{L,\alpha}(\Gamma_s)\}.$$

Recall that if $(g(\boldsymbol{\theta}_{1,i}), \boldsymbol{\theta}_{1,i})$ is on the boundary $\partial\Gamma \cap \partial\Gamma_1$, $\tilde{g}(\boldsymbol{\theta}_{1,i}) = g(\boldsymbol{\theta}_{1,i})$ has no numerical error; otherwise, $\tilde{g}(\boldsymbol{\theta}_{1,i})$ is computed by either the one-dimensional AHSG method discussed in §4.2.1 or one of the root-finding methods discussed in §4.2.2. The approximated hyper-surface $\tilde{\gamma}$ is given by

$$\tilde{\gamma} = \{(\tilde{g}_{L,\alpha}(\boldsymbol{\theta}), \boldsymbol{\theta}) \mid \boldsymbol{\theta} \in \Gamma_s\}.$$

Algorithm 1 is the main algorithm we use to construct our HS-AHSG approximation, where the bisection method is used under the Assumption **A₂**.

By building the approximation $\tilde{g}_{L,\alpha}(\boldsymbol{\theta})$, we decompose a high-dimensional discontinuity detection problem to a set of *one-dimensional* discontinuity detection problems which are much easier to solve than the original problem. Because $g(\boldsymbol{\theta})$ is a

Algorithm 1: *The hyper-spherical adaptive hierarchical sparse-grid approximation*

Initialize $N, L_{\min}, L_{\max}, \alpha, \tau, \mathbf{y}_0$
 $l = -1$
while $l = -1$ or $\left\{ \Delta\mathcal{H}_{L,\alpha}(\Gamma_s) \neq \emptyset \text{ and } l + 1 \leq L_{\max} \right\}$ **do**
 Generate $\Delta\mathcal{H}_{l+1,\alpha}(\Gamma_s)$
 for $\boldsymbol{\theta}_{1,i} \in \Delta\mathcal{H}_{l+1,\alpha}(\Gamma_s)$ **do**
 Search $\boldsymbol{\beta}_{\boldsymbol{\theta}_{1,i}} = (\beta_{\boldsymbol{\theta}_{1,i},1}, \dots, \beta_{\boldsymbol{\theta}_{1,i},N}) \in \Gamma$
 if $f(\boldsymbol{\beta}_{\boldsymbol{\theta}_{1,i}}) = f_1(\boldsymbol{\beta}_{\boldsymbol{\theta}_{1,i}})$ **then**
 $\tilde{g}(\boldsymbol{\theta}_{1,i}) = |\mathbf{y}_0 - \boldsymbol{\beta}_{\boldsymbol{\theta}_{1,i}}|$
 else
 Define $K = \left\lceil \log_2 (|\mathbf{y}_0 - \boldsymbol{\beta}_{\boldsymbol{\theta}_{1,i}}|/\tau) \right\rceil$
 Run bisection $\tilde{g}(\boldsymbol{\theta}_{1,i}) = r_K$ where $|r_K - g(\boldsymbol{\theta}_{1,i})| \leq |\boldsymbol{\beta}_{\boldsymbol{\theta}_{1,i}} - \mathbf{y}_0|/2^K$
 end if
 $\tilde{\omega}_{1,i} = \tilde{g}(\boldsymbol{\theta}_{1,i}) - \tilde{g}_{L,\alpha}(\boldsymbol{\theta}_{1,i})$
 end for
 Update to $\mathcal{H}_{l+1,\alpha}(\Gamma_s)$ by adding $\Delta\mathcal{H}_{l+1,\alpha}(\Gamma_s)$
 $l = l + 1$
end while

smooth function, the mesh refinement may automatically stop at a level $L \leq L_{\max}$. As mentioned in §2, the cost of function evaluations usually dominates the total computational cost. The total cost of constructing the HS-AHSG approximation $\tilde{g}_{L,\alpha}(\boldsymbol{\theta})$ is given by

$$\mathcal{C}_{\text{total}} = \sum_{l=0}^L \sum_{|\mathbf{l}|=l} \sum_{\mathbf{i} \in B_{\Gamma}^{\alpha}} M_{1,\mathbf{i}}^{\tau} \cdot \zeta, \quad (4.5)$$

where ζ is the cost of a single function evaluation of either $f(\mathbf{y})$ or $G(\mathbf{y})$ and $M_{1,\mathbf{i}}^{\tau}$ is the number of function evaluations for obtaining $\tilde{g}(\boldsymbol{\theta}_{1,i})$ with the accuracy τ along the direction $\boldsymbol{\theta}_{1,i}$. Note that $M_{1,\mathbf{i}}^{\tau} = 1$ in the sense that $f(\mathbf{y})$ has the characteristic property and $(g(\boldsymbol{\theta}_{1,i}), \boldsymbol{\theta}_{1,i})$ is on the boundary of Γ . It is well known that the convergence of either the AHSG method or of root-finding methods heavily depends on the size of the search interval. So far, the search interval for each $\boldsymbol{\theta}_{1,i}$ is set to $[S_r(\mathbf{y}_0), S_r(\boldsymbol{\beta}_{\boldsymbol{\theta}})]$

which is the largest possible interval, because we assume that no knowledge about the function value $g(\boldsymbol{\theta}_{1,i})$ is known a priori. In the next section, the efficiency of constructing $\tilde{g}_{L,\alpha}(\boldsymbol{\theta})$ is improved by taking advantage of its hierarchical structure.

4.4. Accelerated approximation using sparse-grid hierarchies. As shown in (4.5), the total computational cost, i.e., the total number of function evaluations, is the summation of the numbers of function evaluations at all sparse-grid points. At each grid point, the number of function evaluations is determined by the prescribed accuracy τ and the initial search interval. So far, the initial search interval for each $\boldsymbol{\theta}_{1,i}$ is set to $[S_r(\mathbf{y}_0), S_r(\boldsymbol{\beta}_{\boldsymbol{\theta}_{1,i}})]$ because we assume no knowledge about the function value $g(\boldsymbol{\theta}_{1,i})$ is known a priori. Such an assumption is true on level $L = 0$. When at a level $L \geq 1$, by the definition of surplus, we have

$$\tilde{g}(\boldsymbol{\theta}_{1,i}) = \tilde{g}_{L-1,\alpha}(\boldsymbol{\theta}_{1,i}) + \tilde{\omega}_{1,i},$$

for each new added point $\boldsymbol{\theta}_{1,i} \in \Delta\mathcal{H}_{L,\alpha}(\Gamma_s)$ on level L . As such, the HS-AHSG approximation of level $L - 1$ can provide a prediction of the function value at each new added point on level L , with the error being the unknown surplus. Such a prediction will become more and more accurate as the surplus decays to zero. Thus, for $L \geq 1$, we utilize the HS-AHSG approximation of the previous level to reduce the size of the initial search interval in order to accelerate the evaluation of $\tilde{g}(\boldsymbol{\theta})$.

Assuming the target function $f(\mathbf{y})$ has the characteristic property, we give the algorithm for the accelerated bisection method in Algorithm 2 which can be extended to other approaches with relative ease.

The basic idea behind Algorithm 2 is to set one of the endpoints, e.g., r_{-1} , of the initial search interval to the predicted value given by the interpolated value $\tilde{g}_{L,\alpha}(\boldsymbol{\theta}_{1,i})$ at the new added point $\boldsymbol{\theta}_{1,i}$. Besides that, several practical issues in terms of efficiency and robustness are considered as well. First, one needs to properly define the other endpoint r_0 such that $|r_{-1} - r_0|$ will become smaller as the level L increases and the interval $[r_{-1}, r_0]$ can cover the discontinuity location $g(\boldsymbol{\theta}_{1,i})$. Theoretically, r_0 can be chosen according to the upper bound of the error $|g(\boldsymbol{\theta}) - \tilde{g}_{L,\alpha}(\boldsymbol{\theta})|$. However, since the a priori error bound is only known up to a constant, in the computations, we use the hierarchical surplus, which acts as an a posteriori error estimate, to choose the other endpoint r_0 . Specifically, for the new added grid points on level L , we initially set the length $|r_{-1} - r_0|$ to the maximum magnitude, denoted by ξ , of all surpluses on level $L - 1$. Note that such surpluses actually characterize the error of the interpolant on level $L - 2$ which means ξ is not the optimal choice, but in most cases, it is big enough to cover the discontinuity and it also decays to zero as L increases. However, in order to avoid the scenario that both r_{-1} and r_0 are on the same side of the discontinuity, e.g., $r_{-1}, r_0 < g(\boldsymbol{\theta})$, we add two loops in Algorithm 2 to recursively enlarge the length $|r_{-1} - r_0|$ by ξ until the interval $[r_{-1}, r_0]$ covers the value $g(\boldsymbol{\theta})$.

4.5. Error estimates and complexity analyses. In this section, we provide error estimates and ε -complexity analyses of the proposed HS-AHSG method for approx-

Algorithm 2: *The accelerated bisection method to compute $\tilde{g}_{l,i} \approx g(\boldsymbol{\theta}_{1,i})$ for $\boldsymbol{\theta}_{1,i} \in \Delta\mathcal{H}_{L,\alpha}(\Gamma_s)$, given $\tilde{g}_{L,\alpha}(\boldsymbol{\theta})$*

$$\xi = \max \left\{ |\omega_{V'V'}| \mid \boldsymbol{\theta}_{V'V'} \in \mathcal{H}_{L-1,\alpha}(\Gamma_s) \text{ and } |V'| = L - 1 \right\}$$

$$\text{Search } \boldsymbol{\beta}_{\boldsymbol{\theta}_{1,i}} = (\beta_{\boldsymbol{\theta}_{1,i},1}, \dots, \beta_{\boldsymbol{\theta}_{1,i},N}) \in \Gamma$$

$$r_{-1} = \min \left\{ \max \{ \tilde{g}_{L-1,\alpha}(\boldsymbol{\theta}_{1,i}), 0 \}, |\mathbf{y}_0 - \boldsymbol{\beta}_{\boldsymbol{\theta}_{1,i}}| \right\}$$

if $f(S^{-1}(r_{-1}, \boldsymbol{\theta}_{1,i})) = f_1(S^{-1}(r_{-1}, \boldsymbol{\theta}_{1,i}))$ **then**

$$r_0 = \min \{ r_{-1} + \xi, |\mathbf{y}_0 - \boldsymbol{\beta}_{\boldsymbol{\theta}_{1,i}}| \}$$

while $f(S^{-1}(r_0, \boldsymbol{\theta}_{1,i})) \neq f_2(S^{-1}(r_0, \boldsymbol{\theta}_{1,i}))$ **do**

$$r_0 = \min \{ r_0 + \xi, |\mathbf{y}_0 - \boldsymbol{\beta}_{\boldsymbol{\theta}_{1,i}}| \}$$

end while

else

$$r_0 = \max \{ r_{-1} - \xi, 0 \}$$

while $f(S^{-1}(r_0, \boldsymbol{\theta}_{1,i})) \neq f_1(S^{-1}(r_0, \boldsymbol{\theta}_{1,i}))$ **do**

$$r_0 = \max \{ r_0 - \xi, 0 \}$$

end while

end if

$$\text{Define } K = \lceil \log_2 (|r_0 - r_{-1}|/\tau) \rceil$$

$$\text{Run bisection } \tilde{g}_{l,i} = r_K \text{ where } |r_K - g(\boldsymbol{\theta}_{1,i})| \leq |r_0 - r_{-1}|/2^K$$

imating the discontinuity hyper-surface γ , i.e., the function $g(\boldsymbol{\theta})$. For simplicity, we assume the target function $f(\mathbf{y})$ satisfies Assumption **A₂**. The analyses are carried out in the context of the isotropic sparse-grid interpolation, given in (3.6), coupled with a bisection method. For the sake of notational convenience, we set $\hat{N} = N - 1$ in the following derivation.

First, it is easy to see that the total error $e = g(\boldsymbol{\theta}) - \tilde{g}_L(\boldsymbol{\theta})$ can be decomposed as

$$e = g(\boldsymbol{\theta}) - \tilde{g}_L(\boldsymbol{\theta}) = \underbrace{g(\boldsymbol{\theta}) - g_L(\boldsymbol{\theta})}_{e_1} + \underbrace{g_L(\boldsymbol{\theta}) - \tilde{g}_L(\boldsymbol{\theta})}_{e_2}, \quad (4.6)$$

where $g_L(\boldsymbol{\theta})$ is the isotropic HS-AHSG approximation of the exact target function

$g(\boldsymbol{\theta})$. An estimate for e is given in the following lemma.

Proposition 4.3. *Under Assumption 4.1, if the transformed function $g(\boldsymbol{\theta})$ has bounded second-order derivatives, i.e., $g(\boldsymbol{\theta}) \in \mathcal{C}^2(\Gamma_s)$, then for the error $e = e_1 + e_2$ in (4.6) we have the estimate*

$$\|e\| \leq C_{\text{sg}} 2^{-2L} \sum_{k=0}^{\widehat{N}-1} \binom{L + \widehat{N} - 1}{k} + 2^{\widehat{N}} \binom{L + \widehat{N}}{\widehat{N}} \tau, \quad (4.7)$$

where τ is the tolerance used for the bisection method, the constant C_{sg} is independent of the level L , and the notation $\|\cdot\|$ denotes the L^∞ norm.

Proof. According to the analyses in [5], the first part e_1 is the error arising from the sparse-grid interpolation which is bounded by

$$\|e_1\| \leq C_{\text{sg}} 2^{-2L} \sum_{k=0}^{\widehat{N}-1} \binom{L + \widehat{N} - 1}{k},$$

where the constant C_{sg} only depends on the dimension \widehat{N} and the upper bound of the L^∞ norm of the second-order derivatives of $g(\boldsymbol{\theta})$. According to the definition in (3.6), the second part e_2 can be written as

$$e_2 = g_L(\boldsymbol{\theta}) - \tilde{g}_L(\boldsymbol{\theta}) = \sum_{l=0}^L \sum_{|\mathbf{l}|=l} (\Delta_{l_1} \otimes \cdots \otimes \Delta_{l_{\widehat{N}}}) (g - \tilde{g})(\boldsymbol{\theta}), \quad (4.8)$$

where $\|g(\boldsymbol{\theta}) - \tilde{g}(\boldsymbol{\theta})\| \leq \tau$. Thus, it is seen that estimating e_2 is equivalent to estimating the Lebesgue constant, denoted by $\Lambda_{\widehat{N},L}$, of the interpolation operator involved. From the representation in (3.6), $\Lambda_{\widehat{N},L}$ can be estimated using triangle inequality, i.e.,

$$\Lambda_{\widehat{N},L} \leq \sum_{l=0}^L \sum_{|\mathbf{l}|=l} \Lambda_{\mathbf{l}} \leq \sum_{l=0}^L \sum_{|\mathbf{l}|=l} \prod_{n=1}^{\widehat{N}} \Lambda_{l_n},$$

where $\Lambda_{\mathbf{l}} = \prod_{n=1}^{\widehat{N}} \Lambda_{l_n}$ is the Lebesgue constant of $\Delta_{l_1} \otimes \cdots \otimes \Delta_{l_{\widehat{N}}}$ and Λ_{l_n} is the Lebesgue constant of Δ_{l_n} . By the definition in (3.2), it is easy to show that

$$\Lambda_{l_n} = \sup \left\{ \frac{\|\Delta_{l_n}(g)\|}{\|g\|} \mid g \text{ is continuous and } g \neq 0 \right\} \leq \lambda_{l_n} + \lambda_{l_n-1},$$

where λ_{l_n} and λ_{l_n-1} are the Lebesgue constants of \mathcal{U}_{l_n} and \mathcal{U}_{l_n-1} , respectively. In the context of linear hierarchical polynomials, we have $\lambda_{l_n} = 1$. Thus, the Lebesgue

constant $\Lambda_{\hat{N},L}$ can be bounded by

$$\begin{aligned}\Lambda_{\hat{N},L} &\leq \sum_{l=0}^L \sum_{|\mathbf{l}|=l} \prod_{n=1}^{\hat{N}} (\lambda_{l_n} + \lambda_{l_{n-1}}) \leq \sum_{l=0}^L \sum_{|\mathbf{l}|=l} 2^{\hat{N}} \\ &= 2^{\hat{N}} \sum_{l=0}^L \binom{l + \hat{N} - 1}{\hat{N} - 1} = 2^{\hat{N}} \sum_{l=0}^L \binom{l + \hat{N} - 1}{l} \\ &= 2^{\hat{N}} \binom{L + \hat{N}}{\hat{N}}.\end{aligned}$$

Thus, the error e_2 in (4.8) can be estimated by

$$\|e_2\| \leq \Lambda_{\hat{N},L} \|g(\boldsymbol{\theta}) - \tilde{g}(\boldsymbol{\theta})\| \leq 2^{\hat{N}} \binom{L + \hat{N}}{\hat{N}} \tau,$$

which concludes the proof. \square

Next, we analyze the cost of constructing $\tilde{g}_L(\boldsymbol{\theta})$ with the prescribed error $\varepsilon > 0$. According to the error estimate in Proposition 4.3, a sufficient condition of $\|e\| = \|g(\boldsymbol{\theta}) - \tilde{g}_L(\boldsymbol{\theta})\| \leq \varepsilon$ is that

$$\|e_1\| \leq C_{\text{sg}} 2^{-2L} \sum_{k=0}^{\hat{N}-1} \binom{L + \hat{N} - 1}{k} \leq \frac{\varepsilon}{2} \quad (4.9)$$

and

$$\|e_2\| \leq 2^{\hat{N}} \binom{L + \hat{N}}{\hat{N}} \tau \leq \frac{\varepsilon}{2}. \quad (4.10)$$

Let \mathcal{C}_{\min} denote the *minimum cost*, i.e., the minimum number of function evaluations, needed to satisfy the inequalities (4.9) and (4.10). The goal is to determine an upper bound for \mathcal{C}_{\min} . Note that, for fixed dimension N and level L , the total cost $\mathcal{C}_{\text{total}}$ is determined by solving the inequality (4.10). The larger is L , the smaller is τ which means, when using the bisection method, a greater number of function evaluations are needed to achieve the accuracy τ . Therefore, the estimation of \mathcal{C}_{\min} has two steps. Given N and ε , we first determine upper bounds for the minimum L needed to achieve (4.9); then, we substitute the obtained value into (4.10) to obtain an upper bound for \mathcal{C}_{\min} .

To perform the first step, we need to estimate the numbers of degrees of freedom of \mathcal{V}_l and \mathcal{W}_l for $l \leq L$, denoted by $|\mathcal{V}_L|$ and $|\mathcal{W}_L|$, respectively. The estimation of $|\mathcal{V}_L|$ has been studied in [5, 11], but the estimate in [11] is not sufficiently sharp and the estimate in [5] has no results related $|\mathcal{W}_L|$. In the following lemma, we provide estimates for $|\mathcal{W}_L|$ which directly leads to an estimate of $|\mathcal{V}_L|$.

Lemma 4.4. *The dimensions of the subspaces \mathcal{W}_l and \mathcal{V}_L for $\widehat{N} \geq 2$, i.e., the numbers of grid points in $\Delta\mathcal{H}_l(\Gamma_s)$ and $\mathcal{H}_L(\Gamma_s)$, respectively, are bounded by*

$$|\mathcal{W}_l| \leq 2^l \binom{l + \widehat{N} - 1}{\widehat{N} - 1} \leq 2^l \left(\frac{l + \widehat{N} - 1}{\widehat{N} - 1} \right)^{\widehat{N} - 1} e^{\widehat{N} - 1}$$

for $0 \leq l \leq L$ and, correspondingly,

$$|\mathcal{V}_L| \leq 2^{L+1} \binom{L + \widehat{N} - 1}{\widehat{N} - 1} \leq 2^{L+1} \left(\frac{L + \widehat{N} - 1}{\widehat{N} - 1} \right)^{\widehat{N} - 1} e^{\widehat{N} - 1}.$$

Proof. Using the (3.6) and exploiting the nesting structure of the sparse grid, the dimension of \mathcal{V}_L can be represented by

$$|\mathcal{V}_L| = \sum_{l=0}^L |\mathcal{W}_l| = \sum_{l=0}^L \sum_{|I|=l} \prod_{n=1}^{\widehat{N}} (m_{l_n} - m_{l_{n-1}}),$$

where $m_{l_n} = 2^{l_n} + 1$ is the number of grid points involved in the one-dimensional interpolant $\mathcal{U}_{l_n}(\cdot)$ in (3.1) and $m_{-1} = 0$. For the linear hierarchical basis, $m_{l_n} - m_{l_{n-1}} = 2^{l_n} - 1$ for $l_n \geq 1$.

We now derive an upper bound for $|\mathcal{W}_l|$ for $l \geq 1$. Note that there are $\binom{\widehat{N}-1+l}{\widehat{N}-1}$ ways to form the sum l with $\widehat{N} - 1 + l$ nonnegative integers, so we have

$$|\mathcal{W}_l| = \prod_{n=1}^{\widehat{N}} (m_{l_n} - m_{l_{n-1}}) \binom{\widehat{N} - 1 + l}{\widehat{N} - 1} \leq 2^l \frac{(\widehat{N} - 1 + l)!}{(\widehat{N} - 1)! \cdot l!}.$$

By an inequality from Stirling's approximation of a factorial, i.e.,

$$d_n \leq n! \leq d_n \left(1 + \frac{1}{4n} \right) \quad \text{with} \quad d_n = \sqrt{2\pi n} \left(\frac{n}{e} \right)^n, \quad n \in \mathbb{N}^+,$$

we obtain that

$$\begin{aligned}
 |\mathcal{W}_l| &\leq 2^l \left(1 + \frac{1}{4(\widehat{N} - 1 + l)} \right) \frac{d_{\widehat{N}-1+l}}{d_{\widehat{N}-1} \cdot d_l} \\
 &= 2^l \frac{\left(1 + \frac{1}{4(\widehat{N} - 1 + l)} \right) \sqrt{\widehat{N} - 1 + l}}{\sqrt{2\pi l(\widehat{N} - 1)}} \left(\frac{\widehat{N} - 1 + l}{\widehat{N} - 1} \right)^{\widehat{N}-1} \left(\frac{\widehat{N} - 1 + l}{l} \right)^l \\
 &\leq 2^l \left(\frac{l + \widehat{N} - 1}{\widehat{N} - 1} \right)^{\widehat{N}-1} \left(1 + \frac{\widehat{N} - 1}{l} \right)^l \\
 &\leq 2^l \left(\frac{l + \widehat{N} - 1}{\widehat{N} - 1} \right)^{\widehat{N}-1} e^{\widehat{N}-1}.
 \end{aligned}$$

It is easy to see that $|\mathcal{W}_0|$ satisfies the above inequality as well. This concludes the proof about $|\mathcal{W}^l|$. The estimate for $|\mathcal{V}_L|$ can be obtained immediately based on the estimate of $|\mathcal{W}_l|$. \square

Next, similar to the analyses in [15], we solve the inequality (4.9) to obtain an upper bound for L such that the error of the isotropic sparse-grid interpolant $g_L(\boldsymbol{\theta})$ is smaller than the prescribed accuracy $\frac{\varepsilon}{2}$.

Lemma 4.5. *For $\varepsilon < 2C_{\text{sg}}$ in (4.9), the accuracy $\|e_1\| \leq \frac{\varepsilon}{2}$ can be achieved with a minimum level L such that*

$$L \leq [L_k] = \left\lceil \frac{t_k \widehat{N}}{2 \ln 2} \right\rceil \quad \text{with} \quad h = \frac{2e}{\ln 2} \left(\frac{2C_{\text{sg}}}{\varepsilon} \right)^{\frac{1}{\widehat{N}}},$$

where $\{t_k\}_{k=0}^{\infty}$ is a monotonically decreasing sequence defined by

$$t_k = \ln(t_{k-1}h) \quad \text{with} \quad t_0 = \frac{e}{e-1} \ln h.$$

Proof. We observe that the value of the minimal solution of the inequality (4.9) has two possibilities, i.e., $L < \widehat{N}$ and $L \geq \widehat{N}$. In the former case, all values larger than \widehat{N} are also solutions of (4.9). Hence, we assume the solution of (4.9) is larger than \widehat{N} . It is also observed that if $L \geq \widehat{N}$, we have

$$\sum_{k=0}^{\widehat{N}-1} \binom{L + \widehat{N} - 1}{k} \leq \widehat{N} \binom{L + \widehat{N} - 1}{\widehat{N} - 1} \leq \widehat{N} \binom{L + \widehat{N}}{\widehat{N}} \leq \widehat{N} \left(\frac{2L}{\widehat{N}} \right)^{\widehat{N}} e^{\widehat{N}}. \quad (4.11)$$

Thus, instead of solving (4.9) directly, it is sufficient to solve

$$C_{\text{sg}} 2^{-2L} \widehat{N} \left(\frac{2L}{\widehat{N}} \right)^{\widehat{N}} e^{\widehat{N}} \leq \frac{\varepsilon}{2} \quad \text{and} \quad L \geq \widehat{N}. \quad (4.12)$$

Now, we temporarily treat L as a positive real number for convenience and the desired iteration number is $\lceil L \rceil$. Let $L = t\widehat{N}/\ln 4$ in (4.12). Then, we have

$$\begin{aligned} & \left(\frac{2L}{\widehat{N}} \right)^{\widehat{N}} e^{\widehat{N}} \left(\frac{2\widehat{N}C_{\text{sg}}}{\varepsilon} \right) \leq 2^{2L} \\ \iff & \left(\frac{t}{\ln 2} \right)^{\widehat{N}} e^{\widehat{N}} \left(\frac{2\widehat{N}C_{\text{sg}}}{\varepsilon} \right) \leq 4^{\frac{t}{\ln 4}\widehat{N}} \\ \iff & \left(\frac{te}{\ln 2} \right) \left(\frac{2\widehat{N}C_{\text{sg}}}{\varepsilon} \right)^{\frac{1}{\widehat{N}}} \leq 4^{\frac{t}{\ln 4}} \\ \iff & \ln t + \ln \left[\frac{e}{\ln 2} \left(\frac{2C_{\text{sg}}}{\varepsilon} \right)^{\frac{1}{\widehat{N}}} \widehat{N}^{\frac{1}{\widehat{N}}} \right] \leq t \\ \iff & \ln t + \ln \left[\frac{2e}{\ln 2} \left(\frac{2C_{\text{sg}}}{\varepsilon} \right)^{\frac{1}{\widehat{N}}} \right] \leq t \end{aligned}$$

so that the inequality (4.12) is satisfied with minimum L given by $L = t\widehat{N}/\ln 4$ if t satisfies

$$t \geq \ln t + \ln h \quad \text{with} \quad h = \frac{2e}{\ln 2} \left(\frac{2C_{\text{sg}}}{\varepsilon} \right)^{\frac{1}{\widehat{N}}},$$

where $h > 1$ by hypothesis. Letting $t_0 = \frac{e}{e-1} \ln h$, it is easy to verify that

$$t_0 - \ln h = \frac{1}{e-1} \ln h \geq 1 + \ln \left(\frac{1}{e-1} \ln h \right) = \ln \left(\frac{e}{e-1} \ln h \right) = \ln t_0,$$

and that the inequality (4.12) is satisfied. Furthermore, for $k \geq 0$, $t_k = \ln(t_{k-1}h) \leq t_{k-1}$ is also the solution of (4.12) due to the fact that

$$\ln t_k + \ln h = \ln(\ln t_{k-1} + \ln h) + \ln h \leq \ln t_{k-1} + \ln h = \ln(t_{k-1}h) = t_k. \quad (4.13)$$

Thus, the sequence $\{t_k\}_{k=0}^{\infty}$ monotonically converges to a unique solution t^* such that $t^* = \ln t^* + \ln h$. Based on the sequence $\{t_k\}_{k=0}^{\infty}$, we can easily find a sequence of upper bounds $\{L_k\}_{k=0}^{\infty}$ for the minimum L satisfying the inequality (4.9). \square

Corollary 4.6. *Under Lemma 4.5, for $k \in \mathbb{N}$, we have*

$$\binom{L_k + \widehat{N}}{\widehat{N}} \leq \frac{\varepsilon}{2\widehat{N}C_{\text{sg}}} \cdot 2^{2L_k}. \quad (4.14)$$

Proof. It is an immediate result by substituting (4.12) into (4.11) \square

We first derive an upper bound for \mathcal{C}_{\min} in the context of the HS-AHSG method without acceleration.

Theorem 4.7. *Under Lemma 4.4 and Lemma 4.5, the minimum total cost \mathcal{C}_{\min} for building the isotropic sparse-grid approximation to $g(\boldsymbol{\theta})$ with accuracy ε based on Algorithm 1 satisfies the estimate*

$$\mathcal{C}_{\min} \leq \zeta \frac{\alpha_1}{\widehat{N}} \left\{ \alpha_2 + \alpha_3 \frac{\log_2 \left(\frac{2C_{\text{sg}}}{\varepsilon} \right)}{\widehat{N}} \right\}^{\alpha_4 \widehat{N}} \left(\frac{2C_{\text{sg}}}{\varepsilon} \right)^{\alpha_5} \left\{ \alpha_6 \log_2 \left(\frac{2C_{\text{sg}}}{\varepsilon} \right) + \alpha_7 \widehat{N} + \alpha_8 \right\},$$

where C_{sg} is the constant in (4.9) and ζ is the cost of one function evaluation of $f(\mathbf{y})$ or $G(\mathbf{y})$ in (2.3). The constants $\alpha_1, \dots, \alpha_8$ are defined by

$$\begin{aligned} \alpha_1 &= 2, & \alpha_2 &= \frac{2e^2}{(e-1)} \log_2 \left(\frac{2e}{\ln 2} \right), & \alpha_3 &= \frac{2e^2}{(e-1)}, & \alpha_4 &= \frac{3}{2}, \\ \alpha_5 &= \frac{1}{2}, & \alpha_6 &= \frac{e}{e-1}, & \alpha_7 &= \frac{e}{e-1} \log_2 \left(\frac{2e}{\ln 2} \right) + 1, & \alpha_8 &= 2 - \log_2(C_{\text{sg}}). \end{aligned} \quad (4.15)$$

Proof. According to the definition in (4.5), the minimum total cost \mathcal{C}_{\min} can be bounded as

$$\mathcal{C}_{\min} \leq \zeta |\mathcal{V}_{L_k}| K(\tau_0, \varepsilon, L_k, \widehat{N}), \quad (4.16)$$

where L_k for $k \in \mathbb{N}$ is determined from Lemma 4.5 and $K(\tau_0, \varepsilon, L, \widehat{N})$ is the necessary number of iterations for the bisection method to achieve the accuracy $\frac{\varepsilon}{2}$ in (4.10) in approximating $g(\boldsymbol{\theta})$ at $\boldsymbol{\theta} \in \Gamma_s$ for fixed \widehat{N} , L , ε , and initial search interval length τ_0 . We can see that the necessary tolerance τ of the bisection method is determined by (4.10), i.e.,

$$\tau(\widehat{N}, L, \varepsilon) = 2^{-\widehat{N}-1} \varepsilon \left/ \binom{L + \widehat{N}}{\widehat{N}} \right.;$$

$K(\tau_0, \varepsilon, L, \widehat{N})$ can be represented by

$$K(\tau_0, \varepsilon, L, \widehat{N}) = \log_2 \left[\frac{2^{\widehat{N}+1} \tau_0}{\varepsilon} \binom{L + \widehat{N}}{\widehat{N}} \right], \quad (4.17)$$

where we temporarily treat K as a positive real number for convenience and the

desired iteration number is $\lceil K \rceil$. According to the discussion in §4.2.2, τ_0 is set to $|\mathbf{y}_0 - \boldsymbol{\beta}_\theta|$ without any prior knowledge, thus $\tau_0 \leq (\widehat{N} + 1)^{\frac{1}{2}}$ which is the length of the diagonal of $[0, 1]^N$. Substituting L_0 into (4.17), we have

$$\begin{aligned}
& K(\tau_0, \varepsilon, L_0, \widehat{N}) \\
& \leq \log_2 \left(\frac{2^{\widehat{N}+1} \tau_0}{\varepsilon} \right) + \log_2 \left(\frac{\varepsilon}{2^{\widehat{N}} C_{\text{sg}}} 2^{2L_0} \right) \\
& = \log_2 \left(\frac{2^{\widehat{N}+1} \tau_0}{C_{\text{sg}} \widehat{N}} \right) + 2L_0 \\
& \leq \log_2 \left(\frac{2^{\widehat{N}+1} (\widehat{N} + 1)^{\frac{1}{2}}}{C_{\text{sg}} \widehat{N}} \right) + \frac{e\widehat{N}}{e-1} \log_2 \left[\frac{2e}{\ln 2} \left(\frac{2C_{\text{sg}}}{\varepsilon} \right)^{\frac{1}{\widehat{N}}} \right] \\
& \leq \widehat{N} + \frac{e\widehat{N}}{e-1} \log_2 \left[\frac{2e}{\ln 2} \left(\frac{2C_{\text{sg}}}{\varepsilon} \right)^{\frac{1}{\widehat{N}}} \right] + 2 - \log_2(C_{\text{sg}}) \\
& = \frac{e}{e-1} \log_2 \left(\frac{2C_{\text{sg}}}{\varepsilon} \right) + \widehat{N} \left\{ \frac{e}{e-1} \log_2 \left(\frac{2e}{\ln 2} \right) + 1 \right\} + 2 - \log_2(C_{\text{sg}}) \\
& = \alpha_6 \log_2 \left(\frac{2C_{\text{sg}}}{\varepsilon} \right) + \alpha_7 \widehat{N} + \alpha_8.
\end{aligned} \tag{4.18}$$

On the other hand, substituting L_1 into the upper bound of \mathcal{V}_{L_1} , we have

$$\begin{aligned}
 |\mathcal{V}_{L_1}| &\leq 2^{L_1+1} \binom{L_1 + \widehat{N} - 1}{\widehat{N} - 1} \leq 2^{L_1+1} \binom{L_1 + \widehat{N}}{\widehat{N}} \\
 &\leq 2^{L_1+1} \left(\frac{\varepsilon}{2\widehat{N}C_{\text{sg}}} \right) 2^{2L_1} \leq \left(\frac{\varepsilon}{\widehat{N}C_{\text{sg}}} \right) 2^{\frac{3t_1\widehat{N}}{2\ln 2}} \\
 &= \left(\frac{\varepsilon}{\widehat{N}C_{\text{sg}}} \right) 2^{\frac{3\ln(t_0h)\widehat{N}}{2\ln 2}} = \left(\frac{\varepsilon}{\widehat{N}C_{\text{sg}}} \right) t_0^{\frac{3}{2}\widehat{N}} \left[\frac{2e}{\ln 2} \left(\frac{2C_{\text{sg}}}{\varepsilon} \right)^{\frac{1}{\widehat{N}}} \right]^{\frac{3}{2}\widehat{N}} \\
 &= \left(\frac{\varepsilon}{\widehat{N}C_{\text{sg}}} \right) \left(\frac{e}{e-1} \ln h \right)^{\frac{3}{2}\widehat{N}} \left(\frac{2e}{\ln 2} \right)^{\frac{3}{2}\widehat{N}} \left(\frac{2C_{\text{sg}}}{\varepsilon} \right)^{\frac{3}{2}\widehat{N}} \\
 &= \frac{2}{\widehat{N}} \left(\frac{2C_{\text{sg}}}{\varepsilon} \right)^{\frac{1}{2}} \left\{ \frac{2e^2}{e-1} \log_2 \left[\frac{2e}{\ln 2} \left(\frac{2C_{\text{sg}}}{\varepsilon} \right)^{\frac{1}{\widehat{N}}} \right] \right\}^{\frac{3}{2}\widehat{N}} \\
 &= \frac{2}{\widehat{N}} \left\{ \frac{2e^2}{e-1} \log_2 \left(\frac{2e}{\ln 2} \right) + \frac{2e^2}{e-1} \frac{\log_2 \left(\frac{2C_{\text{sg}}}{\varepsilon} \right)}{\widehat{N}} \right\}^{\frac{3}{2}\widehat{N}} \left(\frac{2C_{\text{sg}}}{\varepsilon} \right)^{\frac{1}{2}} \\
 &= \alpha_1 \left\{ \alpha_2 + \alpha_3 \frac{\log_2 \left(\frac{2C_{\text{sg}}}{\varepsilon} \right)}{\widehat{N}} \right\}^{\alpha_4 \widehat{N}} \left(\frac{2C_{\text{sg}}}{\varepsilon} \right)^{\alpha_5}.
 \end{aligned} \tag{4.19}$$

Hence, by substituting (4.18) and (4.19) into (4.16), the proof is finished. \square

Next, we analyze the computational cost of the accelerated Algorithm 1 by exploiting Algorithm 2. Unlike the unaccelerated Algorithm 1 for which the length τ_0 of the initial search interval is set to be of the same scale as the domain Γ , in Algorithm 2, for each new added sparse grid point $\boldsymbol{\theta}_{1,\mathbf{i}}$ with $L = |\mathbf{l}| \geq 1$, the desired function value $g(\boldsymbol{\theta}_{1,\mathbf{i}})$ is firstly predicted by the level $L - 1$ HS-AHSG interpolant $\tilde{g}_{L-1}(\boldsymbol{\theta}_{1,\mathbf{i}})$, and then this prediction is used as one endpoint of the initial search interval in the bisection simulation, i.e., $r_{-1} = \tilde{g}_{L-1}(\boldsymbol{\theta}_{1,\mathbf{i}})$. The other endpoint is defined by the upper bound of the error of the prediction, i.e., $|g(\boldsymbol{\theta}_{1,\mathbf{i}}) - \tilde{g}_{L-1}(\boldsymbol{\theta}_{1,\mathbf{i}})|$. In this case, the interval $[r_{-1}, r_0]$ will include the exact function value $g(\boldsymbol{\theta}_{1,\mathbf{i}})$. This is slightly different from the strategy used in Algorithm 2 in which the local error indicator, i.e., the surplus, is used because the upper bound of $|g(\boldsymbol{\theta}_{1,\mathbf{i}}) - \tilde{g}_{L-1}(\boldsymbol{\theta}_{1,\mathbf{i}})|$ is only known up to a constant. In the following derivation, the error bound given in (4.7) is still valid, but, at sparse grid points $\boldsymbol{\theta}_{1,\mathbf{i}}$ for $|\mathbf{l}| = L$, we can obtain a sharper bound for the error of $\tilde{g}_{L-1}(\boldsymbol{\theta})$. The result is provided in the following lemma.

Lemma 4.8. *If the transformed function $g(\boldsymbol{\theta})$ has bounded second-order derivatives, then, at a sparse grid point $\boldsymbol{\theta}_{1,\mathbf{i}}$ with $L = |\mathbf{l}| \geq 1$ and $\mathbf{i} \in B_1(\Gamma_s)$ defined in (3.4),*

the error $g(\boldsymbol{\theta}_{1,i}) - \tilde{g}_{L-1}(\boldsymbol{\theta}_{1,i})$ satisfies the estimate

$$|g(\boldsymbol{\theta}_{1,i}) - \tilde{g}_{L-1}(\boldsymbol{\theta}_{1,i})| \leq C_{\text{surp}} 2^{-2L} + 2^{\hat{N}} \tau,$$

where C_{surp} is independent of L and τ is the tolerance of the bisection algorithm.

Proof. As in (4.7), we split the error into two parts, i.e.,

$$g(\boldsymbol{\theta}_{1,i}) - \tilde{g}_{L-1}(\boldsymbol{\theta}_{1,i}) = \underbrace{g(\boldsymbol{\theta}_{1,i}) - g_{L-1}(\boldsymbol{\theta}_{1,i})}_{e_1} + \underbrace{g_{L-1}(\boldsymbol{\theta}_{1,i}) - \tilde{g}_{L-1}(\boldsymbol{\theta}_{1,i})}_{e_2},$$

where e_1 is the definition of the hierarchical surplus $\omega_{1,i}$ whose upper bound is given in [5], i.e., $|e_1| \leq C_{\text{surp}} \cdot 2^{-2L}$ with C_{surp} is independent of L and e_2 measures the error between the exact prediction of the surplus and the perturbed one. To estimate e_2 , we need to extend the formula for calculating surpluses given in [5] by including the sparse grid points on the boundary. Based on [5, Lemma 3.2], we can see that for each grid point $\boldsymbol{\theta}_{1,i}$ with $|\mathbf{l}| \geq 1$, its exact surplus $\omega_{1,i}$ can be computed from the function values of $g(\boldsymbol{\theta})$ as follows:

$$\omega_{1,i} = \mathcal{A}_{1,i}(g) = \left(\prod_{n=1}^{\hat{N}} \mathcal{A}_{l_n, i_n} \right) (g),$$

where $\mathcal{A}_{1,i}(\cdot)$ is an \hat{N} -dimensional stencil that provides the coefficients for a linear combination of the nodal values of the function g to compute $\omega_{1,i}$. Specifically, $\mathcal{A}_{1,i}$ is product of \hat{N} one-dimensional stencils \mathcal{A}_{l_n, i_n} for $l_n > 0, n = 1, \dots, \hat{N}$, defined by

$$\begin{aligned} \mathcal{A}_{l_n, i_n}(g) &= \left[-\frac{1}{2} \quad 1 \quad -\frac{1}{2} \right]_{l_n, i_n} (g) \\ &= -\frac{1}{2} g(\boldsymbol{\theta}_{1,i} - h_{l_n} \mathbf{e}_n) + g(\boldsymbol{\theta}_{1,i}) - \frac{1}{2} g(\boldsymbol{\theta}_{1,i} + h_{l_n} \mathbf{e}_n), \end{aligned} \tag{4.20}$$

where \mathbf{e}_n is a vector of zeros except for the n -th entry that is one, and h_{l_n} is a scalar equal to a half of the length of the support of the basis function $\psi_{1,i}(\boldsymbol{\theta})$ in the n -th direction. Note that for $l_n = 0$, we have $\mathcal{A}_{l_n, i_n}(g) = [0, 1, 0]_{l_n, i_n}(g)$. It is easy to see that the sum of the absolute values of the coefficients of $\mathcal{A}_{1,i}(\cdot)$ is equal to $2^{\hat{N}}$. Note that all the involved grid points in (4.20) belong to $g_{L-1}(\boldsymbol{\theta})$ except for $\boldsymbol{\theta}_{1,i}$. Thus, due to the fact that $|g(\boldsymbol{\theta}) - \tilde{g}(\boldsymbol{\theta})| \leq \tau$, the error e_2 can be estimated by

$$|e_2| = |\mathcal{A}_{1,i}(g - \tilde{g}) - (g(\boldsymbol{\theta}_{1,i}) - \tilde{g}(\boldsymbol{\theta}_{1,i}))| \leq 2^{\hat{N}} \tau,$$

which concludes the proof. \square

Next, the upper bound of \mathcal{C}_{\min} in the context of using the HS-AHSG method with acceleration is in the following theorem.

Theorem 4.9. *Under Lemma 4.4, 4.5, and 4.8, the minimum total cost \mathcal{C}_{\min} incurred in building the isotropic sparse-grid approximation to $g(\boldsymbol{\theta})$ with accuracy ε using the accelerated HS-AHSG method satisfies the estimate*

$$\mathcal{C}_{\min} \leq \zeta \alpha_1 \left[\alpha_2 + \alpha_3 \frac{\log_2 \left(\frac{2C_{\text{sg}}}{\varepsilon} \right)}{\widehat{N}} \right]^{\alpha_4 \widehat{N}} \left(\frac{2C_{\text{sg}}}{\varepsilon} \right)^{\alpha_5} \left[2\widehat{N} - \log_2(\widehat{N}) + \alpha_9 \right],$$

where C_{sg} is the constant in (4.9) and ζ is the cost of one function evaluation of $f(\mathbf{y})$ or $G(\mathbf{y})$ in (2.3). The constants $\alpha_1, \dots, \alpha_5$ are defined as in Theorem 4.7 and α_9 is defined by

$$\alpha_9 = \log_2 \left(\frac{C_{\text{surp}}}{C_{\text{sg}}} \right) + 2.$$

Proof. For $L = L_1$, according to the definition in (4.5), \mathcal{C}_{\min} can be bounded by

$$\begin{aligned} \mathcal{C}_{\min} &\leq \zeta \sum_{l=0}^{L_1} |\mathcal{W}_l| K(\tau_0^l, \varepsilon, L_1, \widehat{N}) \\ &\leq \zeta \sum_{l=0}^{L_1} 2^l \binom{l + \widehat{N} - 1}{\widehat{N} - 1} \log_2 \left[\frac{2^{\widehat{N}+1} \tau_0^l}{\varepsilon} \binom{L_1 + \widehat{N}}{\widehat{N}} \right], \end{aligned} \quad (4.21)$$

where we temporarily treat K as a positive real number for convenience and the desired iteration number is $\lceil K \rceil$. Based on Lemma 4.8, we define the initial search interval τ_0^l on level l by $\tau_0^l = C_{\text{surp}} 2^{-2l} + 2^{\widehat{N}} \tau$, where τ is the tolerance of the bisection method. For sufficiently small ε , the logarithmic function in (4.21) is positive.

Substituting such τ_0^l into (4.21), we obtain

$$\begin{aligned}
 \mathcal{C}_{\min} &\leq \zeta \sum_{l=0}^{L_1} 2^l \binom{l + \widehat{N} - 1}{\widehat{N} - 1} \log_2 \left[\frac{2^{\widehat{N}+1}}{\varepsilon} \binom{L_1 + \widehat{N}}{\widehat{N}} \left(C_{\text{surp}} 2^{-2l} + 2^{\widehat{N}} \tau \right) \right] \\
 &= \zeta \sum_{l=0}^{L_1} 2^l \binom{l + \widehat{N} - 1}{\widehat{N} - 1} \\
 &\quad \cdot \log_2 \left[\frac{2^{\widehat{N}+1}}{\varepsilon} \binom{L_1 + \widehat{N}}{\widehat{N}} \left(C_{\text{surp}} 2^{-2l} + \frac{\varepsilon}{2 \binom{L_1 + \widehat{N}}{\widehat{N}}} \right) \right] \\
 &= \zeta \sum_{l=0}^{L_1} 2^l \binom{l + \widehat{N} - 1}{\widehat{N} - 1} \left\{ \log_2 \left[\frac{2^{\widehat{N}+1} C_{\text{surp}} 2^{-2l}}{\varepsilon} \binom{L_1 + \widehat{N}}{\widehat{N}} \right] + \widehat{N} \right\} \\
 &\leq \zeta \sum_{l=0}^{L_1} 2^l \binom{l + \widehat{N} - 1}{\widehat{N} - 1} \left\{ \log_2 \left[\frac{2^{\widehat{N}+1} C_{\text{surp}} 2^{2(L_1-l)}}{\varepsilon} \frac{\varepsilon}{2 \widehat{N} C_{\text{sg}}} \right] + \widehat{N} \right\} \\
 &= \zeta \sum_{l=0}^{L_1} 2^l \binom{l + \widehat{N} - 1}{\widehat{N} - 1} \left[2(L_1 - l) + \log_2 \left(\frac{C_{\text{surp}}}{C_{\text{sg}}} \right) + 2\widehat{N} - \log_2(\widehat{N}) \right] \\
 &\leq \zeta \binom{L_1 + \widehat{N}}{\widehat{N}} \sum_{l=0}^{L_1} (L_1 - l) 2^l \\
 &\quad + \zeta 2^{L_1+1} \binom{L_1 + \widehat{N}}{\widehat{N}} \left[\log_2 \left(\frac{C_{\text{surp}}}{C_{\text{sg}}} \right) + 2\widehat{N} - \log_2(\widehat{N}) \right] \\
 &\leq \zeta 2^{L_1+1} \binom{L_1 + \widehat{N}}{\widehat{N}} \left[\log_2 \left(\frac{C_{\text{surp}}}{C_{\text{sg}}} \right) + 2\widehat{N} + 2 - \log_2(\widehat{N}) \right] \\
 &\leq \zeta \alpha_1 \left[\alpha_2 + \alpha_3 \frac{\log_2 \left(\frac{2C_{\text{sg}}}{\varepsilon} \right)}{\widehat{N}} \right]^{\alpha_4 \widehat{N}} \left(\frac{2C_{\text{sg}}}{\varepsilon} \right)^{\alpha_5} \left[2\widehat{N} - \log_2(\widehat{N}) + \alpha_9 \right],
 \end{aligned}$$

which completes the proof. \square

Remark 4.10. Theorem 4.7 and 4.9 tell us that the total cost of the HS-AHSG method is mainly determined by the number of sparse-grid points. Asymptotically, the growth rate of $|\mathcal{V}_L|$ is characterized by the constants α_4 and α_5 , and the cost due to inaccurate initial searching interval is of order $\log_2(1/\varepsilon)$. According to the analyses in [5, 15], the growth rate can be reduced when using high-order hierarchical polynomial bases. In general, with a p -th order hierarchical basis, we have $\alpha_4 = (p+2)/(p+1)$ and $\alpha_5 = 1/(p+1)$. Note that the use of acceleration technique with accurate initial guesses will reduce the total cost by a factor of $\log_2(1/\varepsilon)$ asymptotically, which will be demonstrated in the following section.

5. Numerical examples. In this section, we use three discontinuity detection problems to illustrate the performance of the proposed hyper-spherical adaptive hierarchical sparse-grid method. The first example is used to test the HS-AHSG method in approximating discontinuities of functions with the characteristic property. In the second example, a generic discontinuous function without the characteristic property is considered and the importance of the choice of the origin \mathbf{y}_0 is demonstrated. The third example is an application of the HS-AHSG method in computing the probability of an event that depends on the solution of a partial differential equation with random inputs.

Example 5.1. Consider the three characteristic functions in \mathbb{R}^N

$$F_1(\mathbf{y}) = \begin{cases} 1 & \text{if } \sum_{n=1}^N y_n^2 \geq 1 \\ 0 & \text{otherwise} \end{cases} \quad (5.1)$$

$$F_2(\mathbf{y}) = \begin{cases} 1 & \text{if } |y_3 - y_1| \leq 0.5 \text{ for } \mathbf{y} \in [0, 1]^N \\ 0 & \text{otherwise} \end{cases} \quad (5.2)$$

$$F_3(\mathbf{y}) = \begin{cases} 1 & \text{if } \sqrt{y_1^2 + y_2^2} \leq 0.5 \text{ and } |y_n| < 0.5 \text{ for } n = 3, \dots, N \\ 0 & \text{otherwise,} \end{cases} \quad (5.3)$$

where the characteristic domains of $F_1(\mathbf{y})$, $F_2(\mathbf{y})$, and $F_3(\mathbf{y})$ are a unit hyper-sphere, a layer in the unit hyper-cube, and a hyper-cylinder, respectively. The linear hierarchal basis is used for building the HS-AHSG approximation in the hyper-spherical coordinate system and the bisection method is used to estimate the value of transformed function $g(\boldsymbol{\theta})$ at the sparse-grid points.

First, to illustrate the distribution of the sparse grid points generated by the HS-AHSG method, we set $N = 3$ and plot, in Figures 4, 5 and 6, the discontinuity surface γ , the surface of $g(\boldsymbol{\theta})$, and the sparse-grid points for each $F_1(\mathbf{y})$, $F_2(\mathbf{y})$, and $F_3(\mathbf{y})$, respectively. By comparing Figure 3(b) and Figure 4, we can see the advantage of the HS-AHSG method. The resulting sparse grid contains only 160 points to achieve the desired accuracy whereas the classic AHSG method requires 36,093 grid points. Instead of directly approximating the discontinuous function $F_1(\mathbf{y})$, we approximate the transformed surface shown in Figure 4(b), where its smoothness retains the sparsity of the resulting grid. In Figure 5, we can see that the surface γ is only a part of the boundary $\partial\Gamma_1$ but $\bar{\Gamma}_1$ is a closed subdomain in $\bar{\Gamma}$. There are a total of 1120 sparse grid points on $\partial\Gamma_1$ with only 349 points on γ and 771 points on $\partial\Gamma_1$. According to the discussion in 4.2, at the sparse-grid points placed on $\partial\Gamma_1 \setminus \gamma$, there is no need to run the bisection algorithm to evaluate $g(\boldsymbol{\theta})$ at the 771 points on $\partial\Gamma_1$ so that a significant amount of computational effort is saved. In Figures 5 and 6, we observe that the transformed function $g(\boldsymbol{\theta})$ is not differentiable at the edges and vertices of the charac-

teristic domain Γ_1 so that the HS-AHSG approximation does mesh refinement around these regions. Although the lack of a derivative is not as bad as a jump discontinuity, it may result in a failure of the HS-AHSG method if the volume of such a singularity grows fast as the dimension N increases. This issue will be considered in future work.

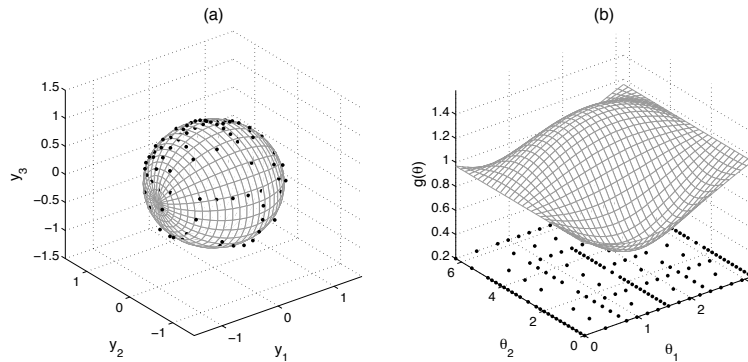


Figure 4: (a) The discontinuity surface γ with sparse-grid points; (b) the transformed surface $g(\boldsymbol{\theta})$ in the hyper-spherical coordinate system. The parameters for the HS-AHSG approximation are $L_{\min} = 4$, $L_{\max} = 12$, $\alpha = 0.01$, and $\mathbf{y}_0 = (0.1, 0.2, 0.3)$; the total number of sparse-grid points is 160.

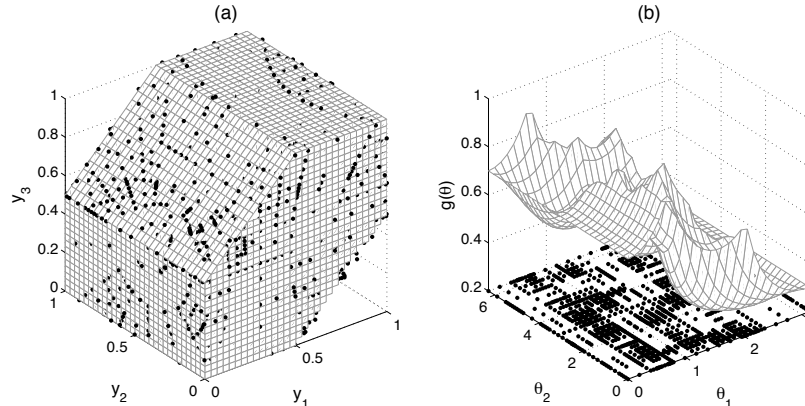


Figure 5: (a) The discontinuity surface γ with sparse-grid points; (b) the transformed surface $g(\boldsymbol{\theta})$ in the hyper-spherical coordinate system. The parameters for the HS-AHSG approximation are $L_{\min} = 4$, $L_{\max} = 12$, $\alpha = 0.01$, and $\mathbf{y}_0 = (0.3, 0.4, 0.5)$; the total number of sparse-grid points is 1120 of which only 349 are off the boundary.

Next, we test the convergence of the HS-AHSG method in detecting the discontinuity of $F_1(\mathbf{y})$ in three cases: the HS-AHSG method with isotropic sparse grids and no acceleration, the HS-AHSG method with isotropic sparse grids and acceleration, and the HS-AHSG method with adaptive sparse grids and acceleration. The origin of the hyper-spherical coordinate system is set to $\mathbf{y}_0 = (0.2/\sqrt{N}, \dots, 0.2/\sqrt{N})$ which is

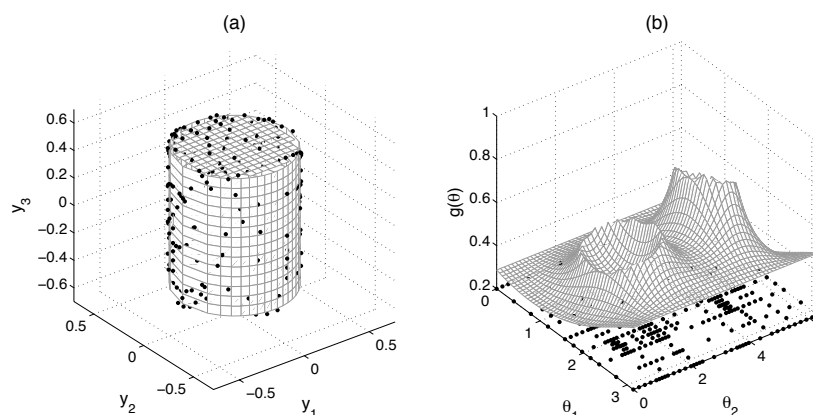


Figure 6: (a) The discontinuity surface γ with sparse-grid points; (b) the transformed surface $g(\boldsymbol{\theta})$ in the hyper-spherical coordinate system. The parameters for the HS-AHSG approximation are $L_{\min} = 4$, $L_{\max} = 12$, $\alpha = 0.01$, and $\mathbf{y}_0 = (0.1, 0.1, 0.1)$; the total number of sparse-grid points is 473.

0.2 away from the origin $(0, \dots, 0)$. The error decay for $N = 2, 3, 4, 5, 7, 9$ is plotted in Figure 7. As expected, for high-dimensional discontinuity detection, our approach achieves faster convergence rates than the well known AHSG method. Moreover, for the same accuracy, acceleration and adaptivity can provide a significant saving in computational cost. Further evidence of this is seen in Table 2 for which the computational cost is again measured by the total number of function evaluations.

Example 5.2. Consider the two-dimensional discontinuous function on $[-1.5, 1.5] \times [-1.5, 1.5]$ given by

$$f(\mathbf{y}) = \begin{cases} y_1^2 + y_2^2 & \text{if } \sqrt{y_1^2 + y_2^2} \leq 1 + \frac{1}{4} \cos\left(4 \arctan\left(\frac{y_2}{y_1}\right)\right) \\ y_1^2 + y_2^2 + \frac{1}{2} & \text{otherwise} \end{cases} \quad (5.4)$$

which is plotted in Figure 8, where the jump discontinuity is along the curve $\sqrt{y_1^2 + y_2^2} = 1 + \frac{1}{4} \cos(4 \cdot \arctan(y_2/y_1))$. We observe that the domain Γ_1 defined as the interior of this curve is star-convex but is not convex so that only a subset of points in Γ_1 can be used as the origin of the hyper-spherical coordinate system. We test our approach with the origin being $(0, 0)$ and $(-1.1, 0)$ and the bisection method is used to approximate the transformed function $g(\boldsymbol{\theta})$. The captured discontinuity curves and the corresponding transformed curves are plotted in Figure 8(b) and 8(c), respectively. It is easy to see that the point $(0, 0)$ is a qualified point to be the origin of the polar system so that the approximate curve captures the discontinuity very well. In contrast, $(-1.1, 0)$ does not satisfy the Assumption 4.1 so that the function $f_{\boldsymbol{\theta}}(r)$ has multiple roots along some directions whereas the bisection algorithm can only find one root. Thus, the discontinuity curve is not captured correctly in a subdomain of Γ_s , as shown in Figure

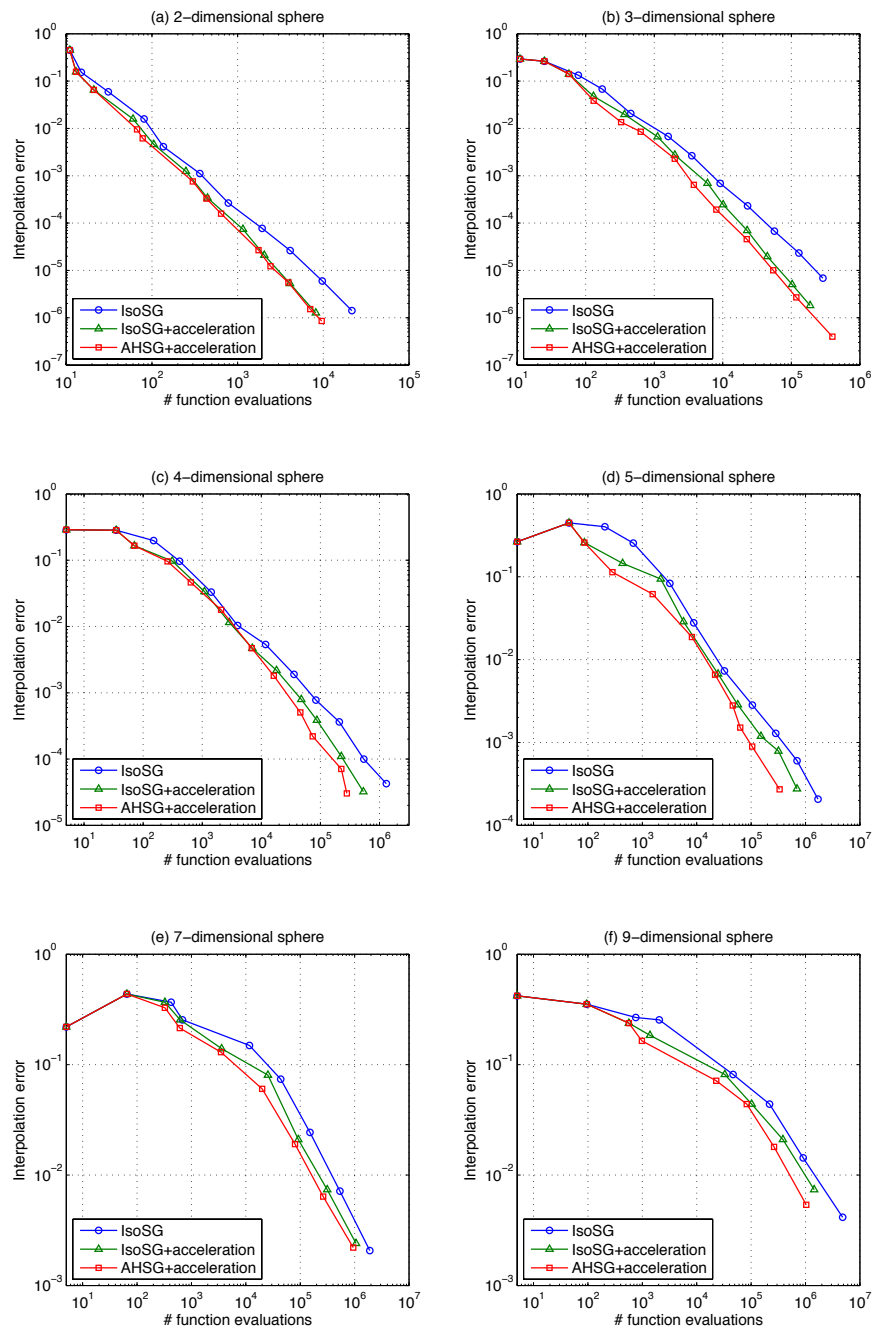


Figure 7: Error decay of the HS-AHSG method with isotropic sparse grids and no acceleration, isotropic sparse grids and acceleration, and adaptive sparse grids and acceleration for detecting the discontinuity of $f_1(\mathbf{y})$ in Example 5.1 with $L_{\min} = 4$, $L_{\max} = 12$, $\mathbf{y}_0 = (0.2/\sqrt{N}, \dots, 0.2/\sqrt{N})$ for $N = 2, 3, 4, 5, 7, 9$

8(b).

Table 2: Computational costs and savings of the HS-AHSG method with acceleration and adaptivity in Example 5.1

Dim	Error	IsoSG cost	IsoSG+acceleration		AHSG+acceleration	
			cost	saving	cost	saving
2D	1.0e-3	384	274	28.7%	251	34.7%
	1.0e-4	1,603	955	40.4%	832	48.1%
	1.0e-5	7,230	2,968	58.9%	2,737	62.1%
3D	1.0e-3	7,046	4,461	36.7%	3,022	57.1%
	1.0e-4	42,541	18,021	57.6%	12,817	69.9%
	1.0e-5	224,978	67,721	69.9%	54,439	75.8%
4D	5.0e-2	880	682	22.5%	584	33.6%
	1.0e-3	66,207	38,165	42.4%	26,329	60.2%
	1.0e-4	542,632	241,337	55.5%	161,354	70.3%
5D	5.0e-2	5,135	3,645	29.0%	2,082	59.5%
	1.0e-2	23,782	16,558	30.4%	14,694	38.2%
	1.0e-3	383,884	207,862	45.9%	94,148	75.5%
7D	1.0e-1	24,757	11,770	52.5%	6,327	74.4%
	5.0e-2	67,671	40,221	40.6%	25,111	62.9%
	5.0e-3	773,113	479,984	37.9%	354,040	54.2%
9D	1.0e-1	26,593	14,843	44.2%	6,426	75.8%
	5.0e-2	157,851	80,507	49.0%	58,849	62.7%
	1.0e-2	1,472,441	983,101	33.2%	513,163	65.1%

In addition, if we assume the function $f(\mathbf{y})$ has no characteristic property, the one-dimensional AHSG approach discussed in §4.2.1 has to be used to estimate the value of the transformed function $g(\boldsymbol{\theta})$. For comparison, in Figure 9(a-b), we plot the points at which the function $f(\mathbf{y})$ is evaluated to estimate the transformed function $g(\boldsymbol{\theta})$ at the first 17 sparse grid points in Γ_s . As expected, the one-dimensional AHSG method requires 532 function evaluations whereas the bisection method only requires 242 function evaluations. Further proof can be seen in Figure 9(c) where the decays of the interpolation errors are plotted. When setting the origin $\mathbf{y}_0 = (-1.1, 0)$, the error does not decay toward zero because of the violation of Assumption 4.1. When $\mathbf{y}_0 = (0, 0)$, we can see that the use of the characteristic property and the hierarchical acceleration can significantly reduce the number of function evaluations to achieve the prescribed accuracy.

Example 5.3. Consider a two-dimensional steady heat equation with stochastic

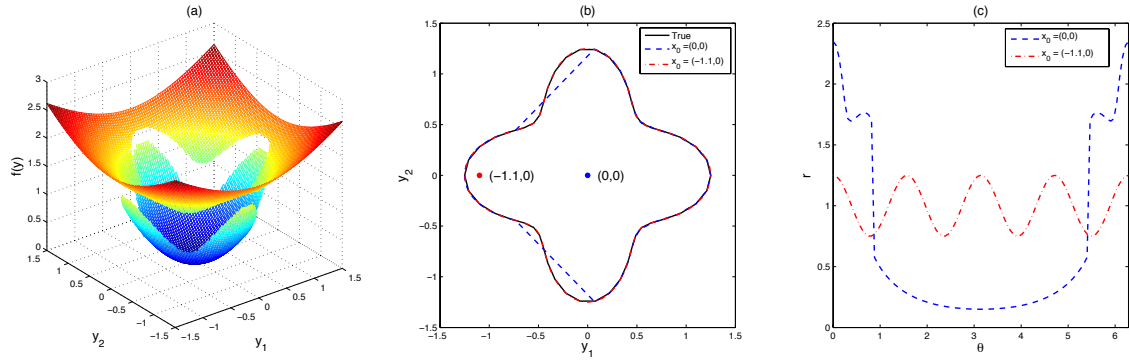


Figure 8: (a) The surface of the target function $f(\mathbf{y})$ in Example 5.2; (b) the true discontinuity curve and the approximated curves with the origin of the polar coordinate system being $(0, 0)$ and $(-1.1, 0)$; (c) the transformed functions of the discontinuity curves in the polar coordinate system.

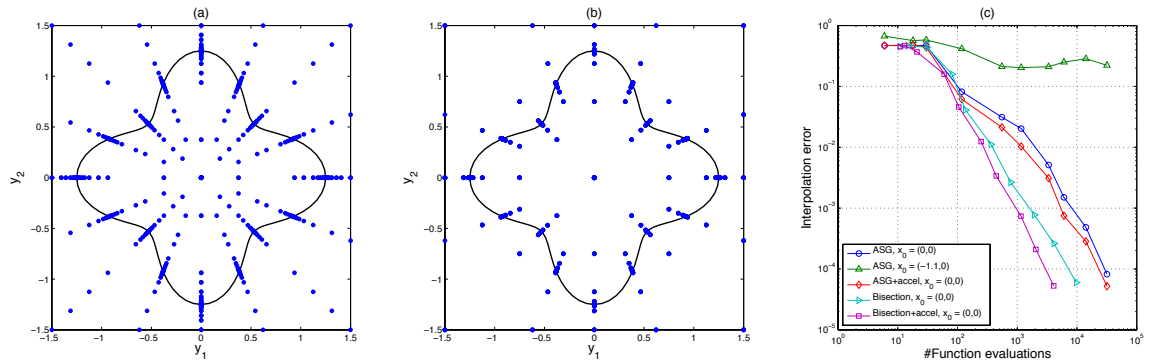


Figure 9: (a) The 532 points (blue dots) at which the function $f(\mathbf{y})$ without the characteristic property is evaluated to estimate the transformed function $g(\boldsymbol{\theta})$ at the first 17 sparse-grid points in the polar coordinate system; (b) the 242 points (blue dots) at which the function $f(\mathbf{y})$ with the characteristic property is evaluated to estimate the transformed function $g(\boldsymbol{\theta})$ at the first 17 sparse-grid points in the polar coordinate system; (c) the decay of the interpolation error.

diffusivity

$$\begin{cases} \nabla \cdot (\kappa(x, \omega) \nabla u(x, \omega)) = h(x) \text{ in } [0, 1]^2 \times \Omega, \\ u(x, \omega) = 0 \text{ on } \partial D \times \Omega \end{cases} \quad (5.5)$$

with

$$h(x) = 2000 + \exp\left(-\frac{(x_1 - 0.6)^2 + (x_2 - 0.8)^2}{0.05^2}\right) \quad (5.6)$$

and

$$\kappa(x, \omega) = y_1(\omega)^2 + \exp \left[y_2(\omega)^4 \sin(\pi x_1) + y_3(\omega)^2 \sin(\pi x_2) + \cos(\pi x_1) + \cos(\pi x_2) \right], \quad (5.7)$$

where $\mathbf{y}(\omega) = (y_1(\omega), y_2(\omega), y_3(\omega))$ are independent and identically distributed random variables following the uniform distribution $U([-1, 1])$. The quantity of interest is the probability of the event that the integral of the solution $u(x, \omega)$ over D is larger than the threshold value 1.2, i.e.,

$$QoI = \int_{\Omega} \mathcal{X}_{\Gamma_1}(\mathbf{y}) \rho(\mathbf{y}) d\mathbf{y} \quad \text{where} \quad \Gamma_1 = \mathbb{P} \left\{ \mathbf{y} \in \mathbb{R}^3 \mid \int_D u(x, \mathbf{y}(\omega)) dx > 1.2 \right\}. \quad (5.8)$$

where Γ_1 is the domain of interest and the characteristic function $\mathcal{X}_{\Gamma_1}(\mathbf{y})$ is discontinuous across the boundary $\gamma = \partial\Gamma_1$. Note that this example satisfies the Assumption **A₃** given in §2 and the implicit function is defined by $G(\mathbf{y}) = 1.2 - \int_D u(x, \mathbf{y}) dx = 0$ which is smooth due to the regularity of the solution u . In this case, we can use more advanced root-finding methods as discussed in §4.2.2, such as the Regula Falsi method. Here we use the HS-AHSG method with both acceleration and adaptivity and only compare the performances of different root-finding methods. The origin of the hyper-spherical coordinate system is set to $(0.01, 0.2, 0.05)$. The surface γ and its transformed representation are plotted in Figure 10(a) and 10(b), respectively. For $L_{\min} = 3$, $L_{\max} = 20$, and $\alpha = 0.01$, we end up with a total of 344 sparse-grid points in the hyper-spherical domain Γ_s ; those points are also plotted in Figure 10(a) and 10(b). In Figure 10(c), we show the error decay of the HS-AHSG approximations using the bisection and Regula Falsi methods, respectively. It is easy to see that the Regula Falsi method can provide additional savings in computational costs over the bisection method by taking advantage of the availability and smoothness of $G(\mathbf{y})$. Further evidence of this can be seen in Table 3.

Table 3: The computational cost of the HS-AHSG method using the bisection method and the Regula Falsi method in Example 5.3

Error	Bisection	Regula Falsi	Saving
1.0e-3	4,116	3,381	17.8%
1.0e-4	17,464	13,047	25.3%
1.0e-5	68,299	48,555	28.9%

6. Conclusions. In this paper, we propose a comprehensive methodology for high-dimensional discontinuity detection by extending well-known sparse-grid methods. Both theoretical and numerical results demonstrate that our approach is a sig-

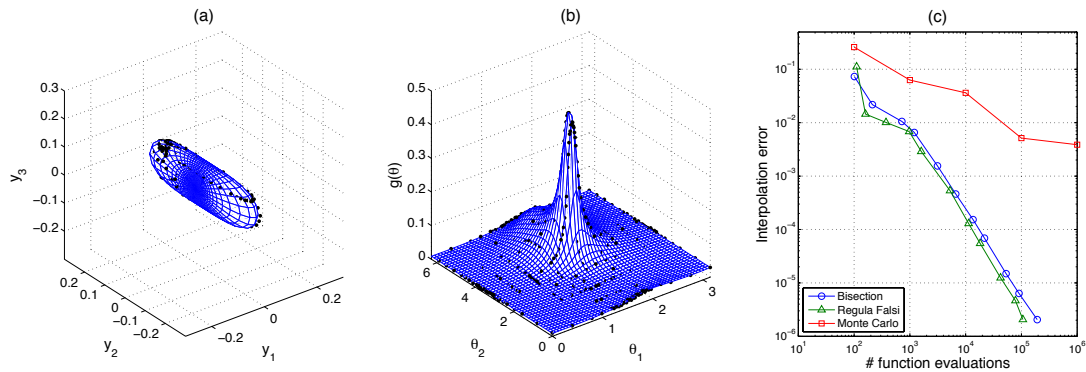


Figure 10: (a) The discontinuity surface γ with 344 sparse grid points; (b) the transformed surface $g(\boldsymbol{\theta})$ in the hyper-spherical coordinate system. The parameters for the HS-AHSG approximation are $L_{\min} = 4$, $L_{\max} = 12$, $\alpha = 0.01$, and $\mathbf{y}_0 = (0.01, 0.2, 0.05)$. (c) The error decays of the Monte Carlo method and the HS-AHSG approximation using the bisection and the Regula Falsi methods.

nificant improvement to existing methods. Moreover, our approach is not restricted to the context of sparse-grid approximation. It can be combined with any other numerical method for high-dimensional approximation such as radial basis approximation and mesh-free interpolations. In future work, we will focus on how to relax the assumption related to the geometry of the domain of interest, so that problems with more complicated geometries can be investigated.

Acknowledgements. The first author was by the Department of Energy Advanced Simulation Computing Research (ASCR), through the Householder Fellowship at the Oak Ridge National Laboratory (ORNL). The ORNL is operated by UT-Battelle, LLC, for the United States Department of Energy under Contract DE-AC05-00OR22725. The second author was by the US Department of Defense Air Force Office of Scientific Research (AFOSR) under grant number 1854-V521-12 and US Department of Energy ASCR under grant number ERKJ259. The third author was supported by the US Department of Defense AFOSR under grant number FA9550-11-1-0149 and by the US Department of Energy ASCR under grant number DE-SC0010678.

REFERENCES

- [1] R. ARCHIBALD, A. GELB, R. SAXENA, AND D. XIU, *Discontinuity detection in multivariate space for stochastic simulations*, *J. Comput. Phys.*, 228 (2009), pp. 2676–2689.
- [2] R. ARCHIBALD, A. GELB, AND J. YOON, *Polynomial fitting for edge detection in irregularly sampled signals and images*, *SIAM J. Numer. Anal.*, 43 (2005), pp. 259–279 (electronic).

- [3] I. BABUSKA, F. NOBILE, AND R. TEMPONE, *A stochastic collocation method for elliptic partial differential equations with random input data*, SIAM J. Numer. Anal., 45 (2007), pp. 1005–1034.
- [4] H. J. BUNGARTZ AND S. DIRNSTORFER, *Multivariate Quadrature on Adaptive Sparse Grids*, Computing, 71 (2003), pp. 89–114.
- [5] H.-J. BUNGARTZ AND M. GRIEBEL, *Sparse grids*, Acta Numerica, 13 (2004), pp. 1–123.
- [6] M. GUNZBURGER, C. WEBSTER, AND G. ZHANG, *An Adaptive Wavelet Stochastic Collocation Method for Irregular Solutions of Partial Differential Equations with Random Input Data*, Springer Lecture Notes on Computational Science and Engineering, (2014), p. to appear.
- [7] —, *Stochastic Finite Element Methods for Partial Differential Equations with Random Input Data*, Acta Numerica, (2014), p. to appear.
- [8] J. D. JAKEMAN, R. ARCHIBALD, AND D. XIU, *Characterization of discontinuities in high-dimensional stochastic problems on adaptive sparse grids*, J. Comput. Phys., 230 (2011), pp. 3977–3997.
- [9] P. JANTSCH, C. WEBSTER, AND G. ZHANG, *A Hierarchical Stochastic Collocation Method for Adaptive Acceleration of PDEs with Random Input Data*, tech. rep., Oak Ridge National Laboratory, 2014.
- [10] X. MA AND N. ZABARAS, *An adaptive hierarchical sparse grid collocation algorithm for the solution of stochastic differential equations*, J. Comput. Phys., 228 (2009), pp. 3084–3113.
- [11] F. NOBILE, R. TEMPONE, AND C. G. WEBSTER, *A sparse grid stochastic collocation method for partial differential equations with random input data*, SIAM J. Numer. Anal., 46 (2008), pp. 2309–2345.
- [12] —, *An anisotropic sparse grid stochastic collocation method for partial differential equations with random input data*, SIAM J. Numer. Anal., 46 (2008), pp. 2411–2442.
- [13] B. ØKSENDAL, *Stochastic Differential Equations: An Introduction with Applications (Universitext)*, Springer, 6th ed., 2010.
- [14] A. QUARTERONI, R. SACCO, AND F. SALERI, *Numerical Mathematics*, Springer Verlag, 2007.
- [15] G. W. WASILKOWSKI AND H. WOŹNIAKOWSKI, *Explicit cost bounds of algorithms for multivariate tensor product problems*, J. Complexity, 11 (1995), pp. 1–56.
- [16] D. XIU AND J. S. HESTHAVEN, *High-Order Collocation Methods for Differential Equations with Random Inputs*, SIAM J. Sci. Comput., 27 (2005), pp. 1118–1139.
- [17] D. XIU AND G. E. KARNIADAKIS, *The Wiener-Askey polynomial chaos for stochastic differential equations*, SIAM J. Sci. Comput., 24 (2002), pp. 619–644 (electronic).
- [18] G. ZHANG AND M. GUNZBURGER, *Error Analysis of A Stochastic Collocation Method for Parabolic Partial Differential Equations with Random Input Data*, SIAM J. Numer. Anal., 50 (2012), pp. 1922–1940.

- [19] G. ZHANG, M. GUNZBURGER, AND W. ZHAO, *A sparse-grid method for multi-dimensional backward stochastic differential equations*, Journal of Computational Mathematics, 31 (2013), pp. 221–248.
- [20] G. ZHANG, D. LU, M. YE, M. GUNZBURGER, AND C. WEBSTER, *An adaptive sparse-grid high-order stochastic collocation method for bayesian inference in groundwater reactive transport modeling*, Water Resources Research, 49 (2013), pp. 6871–6892.

